

General Relativistic Effects in the Core Collapse Supernova Mechanism

S. W. Bruenn¹ and K. R. De Nisco

Department of Physics, Florida Atlantic University, Boca Raton, FL 33431-0991

and

A. Mezzacappa¹

Physics Division, Oak Ridge National Laboratory, Oak Ridge, TN 37831-6354

Received _____; accepted _____

¹Institute for Theoretical Physics, University of California at Santa Barbara, Santa Barbara, CA 94913

ABSTRACT

We apply our recently developed code for spherically symmetric, fully general relativistic (GR) Lagrangian hydrodynamics and multigroup flux-limited diffusion (MGFLD) neutrino transport to examine the effects of GR on the hydrodynamics and transport during collapse, bounce, and the critical shock reheating phase of core collapse supernovae. GR effects were examined by performing core collapse simulations from several precollapse models in the Newtonian limit, in a hybrid limit consisting of GR hydrodynamics and Newtonian transport, and in the fully GR limit. Comparisons of models computed with GR versus Newtonian hydrodynamics show that collapse to bounce takes slightly less time in the GR limit, and that the shock propagates slightly farther out in radius before receding. After a secondary quasistatic rise in the shock radius, the shock radius declines considerably more rapidly in the GR simulations than in the corresponding Newtonian simulations. During the shock reheating phase, core collapse computed with GR hydrodynamics results in a substantially more compact structure from the center out to the stagnated shock, the shock radius being reduced by a factor of 2 after 300 ms for a $25 M_{\odot}$ model and 600 ms for a $15 M_{\odot}$ model, times being measured from bounce. The inflow speed of material behind the shock is also increased by about a factor of 2 throughout most of the evolution as a consequence of GR hydrodynamics. Regarding neutrino transport, comparisons show that the luminosity and rms energy of any neutrino flavor during the shock reheating phase increases when switching from Newtonian to GR hydrodynamics. This arises from the close coupling of the hydrodynamics and transport and the effect of GR hydrodynamics to produce more compact core structures, hotter neutrinospheres at smaller radii. On additionally switching from Newtonian to GR transport, gravitational time dilation and redshift effects

decrease the luminosities and rms energies of all neutrino flavors. This decrease is less in magnitude than the increase in neutrino luminosities and rms energies that arise when switching from Newtonian to GR hydrodynamics, with the result that a fully GR simulation gives higher neutrino luminosities and harder neutrino spectra than a fully Newtonian simulation of the same precollapse model. We conclude with a discussion of some implications of these results regarding the development of neutrino-driven convection during the shock reheating phase, and supernova nucleosynthesis.

Subject headings: (stars:) supernovae: general – neutrinos – general relativity

1. Introduction

Realistic simulations of stellar core collapse, by which we include the core collapse supernova mechanism, the collapse of stellar cores to black holes, the cooling and deleptonization of nascent neutron stars, the modeling of neutrino-driven winds, and the prediction of neutrino signatures, requires the implementation of accurate numerical radiation-hydrodynamics over extremes of temperature, density, and neutrino luminosities. The wide range of outcomes obtained by different groups engaged in simulating the core collapse supernova mechanism, for example, is testimony to the difficulty of numerically modeling this multicomponent and highly nonlinear phenomenon.

In this paper, we draw attention to the importance of incorporating general relativity in simulations of stellar core collapse, with particular focus on the core collapse supernova mechanism. General relativity must be an essential component in the realistic modeling of this mechanism because of the very strong gravitational fields that arise. (Hereafter GR will be used to denote both the noun “general relativity” and the adjective “general relativistic.”)

The core collapse supernova mechanism is still unknown and involves a complex interplay of hydrodynamics and neutrino transport, both of which can be significantly modified by GR effects in the crucial period during which the explosion develops. For example, GR effects can be expected to substantially modify the hydrodynamics of the core at high densities. An extreme example of this, of course, is the possibility that in the GR limit one can have continued collapse and the formation of an event horizon. The neutrino transport will also be modified by GR, directly through redshift, time dilation, curvature, and aberration effects, and indirectly through its strong coupling to the GR modified hydrodynamics.

Other aspects of stellar core collapse will benefit from improved radiation-hydrodynamics codes. The detection of neutrinos from supernova 1987A (Bionta et al. 1987; Hirata et al. 1987) opened up a new window on the Universe, through which we can observe deep inside the core of a massive star as it goes through its death throes. There are now a number of large underground particle detectors, currently on line, such as Super Kamiokande (SuperK) (Totsuka 1992; Nakamura et al. 1994a,b) and the Sudbury Neutrino Observatory (SNO) (Ewan 1992, 1996; Sur 1994; Moorhead 1997), or detectors being constructed that will be very sensitive to the neutrino radiation from a core collapse occurring within the Milky Way galaxy, and sensitive enough to detect neutrinos from a core collapse occurring anywhere within the Local Group. The information coded in the neutrino fluxes from a Galactic supernova will be voluminous, shedding light on the supernova mechanism, and possibly on the fundamental properties of neutrinos themselves, i.e., whether they have masses and are mixed. Simulations of the energetics and timescales of the neutrino emission in all flavors, incorporating GR hydrodynamics and multigroup neutrino transport, will be essential for extracting important features concerning the physics of stellar core collapse and the fundamental properties of neutrinos from the neutrino signatures recorded by the new terrestrial detectors.

Previous work at various levels has been done on the problem of coupling the GR equations of gravity, hydrodynamics, and radiation transport in spherical symmetry. Lindquist (1966) obtained the general form of the GR Boltzmann equation and its explicit form and the form of the equations for the first two energy integrated angular moments in a spherical coordinate system in a diagonal gauge (i.e., with a zero shift vector). (This was the coordinate system used, for example, by Misner & Sharp (1965) and by May & White (1966) in their derivation of the GR hydrodynamics equations.) These equations were also presented by Baron et al. (1989), who additionally presented the explicit form of the equations for the first two monochromatic angular moments. Mayle (1985), Schinder (1988), and Mezzacappa & Matzner (1989) derived the GR Boltzmann equation for nondiagonal gauges, which have desirable singularity-avoidance properties; Schinder (1988) additionally derived the monochromatic and energy-integrated neutrino distribution zeroth and first angular moment equations.

The first fully GR numerical simulation of stellar core collapse, with the aim of modeling the supernova mechanism, was performed by Schwartz (1967), who coupled GR hydrodynamics in the diagonal gauge with equilibrium diffusion for the neutrino transport. This was followed by more elaborate stellar core collapse simulations by Wilson (1971), who developed a code coupling GR hydrodynamics and GR Boltzmann transport, again in the diagonal gauge, but utilizing much simplified (compared to more recent simulations) neutrino physics (e.g., all neutrino scatterings were treated as absorptions). Other codes were subsequently constructed to simulate stellar core collapse with some implementation of GR—Bowers & Wilson (1982) (post-Newtonian hydrodynamics, some order v/c effects in neutrino transport), Van Riper & Lattimer (1981); Van Riper (1982) (GR Hydrodynamics), Bruenn (1985) (GR Hydrodynamics, transport of order v/c), Mayle (1985) (post-Newtonian hydrodynamics, gravitational redshifting of neutrinos), Myra & Bludman (1989) (GR hydrodynamics, gravitational redshifting of neutrinos), Cooperstein

et al. (1986) (hydrodynamics and neutrino transport to order v/c), Fryer et al. (1999); Fryer (1999) (GR hydrodynamics), Bruenn et al. (2000a) (GR hydrodynamics and transport) Liebendörfer et al. (2000) (GR hydrodynamics and transport).

While the above indicates that a number of codes have been constructed which implement GR at various levels of approximation (and which implement neutrino transport at various levels of approximation), direct comparisons between Newtonian and GR simulations are few. An exception to this occurred during the period from the late 1970’s through most of the 1980’s. During this period a viable explosion mechanism, referred to as the “prompt mechanism”, was thought to be a purely hydrodynamic one wherein the collapsing core on regaining dynamic stability at nuclear densities overshoots its new equilibrium position and then rebounds to a larger radius. During rebound, the expanding core acts like a spherical piston and generates a shock wave which propagates into the overlaying matter. While the generation of a shock wave on core bounce is a generic feature of core collapse, the prompt mechanism requires that this shock be strong enough to directly propagate outward through the mantle, reverse the velocity of the material there, and eject the outer layers of the star explosively, thereby “promptly” causing the supernova explosion. Critical to the prompt mechanism is the initial strength of the bounce shock and the mass of the outer core through which it must propagate before entering the mantle. This, in turn, was found to depend sensitively on the equation of state and on the use of GR hydrodynamics (Van Riper 1978; Van Riper & Arnett 1978; Van Riper 1979; Baron et al. 1985, 1987; Van Riper 1988; Swesty et al. 1994). Comparisons of Newtonian versus GR simulations of core infall and bounce show that the stronger “gravitational attraction” of GR and its tendency to reduce the difference above nuclear density between the effective adiabatic index of the matter and the critical adiabatic index causes the GR simulations to produce higher density bounces, larger rebound amplitudes, and stronger initial shocks.

The failure of the prompt mechanism to produce explosions when modeled with accurate neutrino transport (except possibly for a very limited region of core masses and equation of state parameters) and the inability of spherically symmetric simulations to produce explosions at later times caused much of the research on the core collapse supernova mechanism in the early to mid 1990’s to shift to the role of multidimensional effects, and in particular, convection. This focus on convection was motivated in part by the potential of convection for increasing the likelihood of explosions, and in part by a number of observations of SN 1987A, which indicate that extensive mixing occurred throughout much of the ejected material, pointing, *by inference*, to fluid instabilities arising during the explosion itself. These investigations have employed multidimensional simulations with Newtonian hydrodynamics and transport (Herant, Benz, & Colgate 1992; Herant et al. 1994; Miller, Wilson, & Mayle 1993; Janka & Müller 1996a,b; Burrows, Hayes, & Fryxell 1995; Mezzacappa et al. 1998a,b). While this work is extremely important, it has ignored the role of GR.

Recent developments in core collapse supernovae theory (e.g., the possibility of r-process nucleosynthesis in neutrino driven winds, further investigations of convection and rotation) have resulted in a growing number of simulations performed with the incorporation of various levels of GR. This, together with the restriction of previous comparisons of Newtonian and GR simulations to infall and bounce, and to the hydrodynamic sector of these simulations, has motivated us to extend these comparisons to the core evolution well beyond bounce and to the neutrino transport sector of the simulations as well.

Two fully GR radiation-hydrodynamic codes have recently been developed which implement multigroup neutrino transport. One code, *BOLTZTRAN-AGILE*, developed by Liebendörfer (2000), couples GR hydrodynamics, GR Boltzmann neutrino transport, and the Einstein equations. This code is a marriage of an adaptive mesh, conservative GR

hydrodynamic code (Liebendörfer 2000) with a three-flavor Boltzmann neutrino transport solver (Mezzacappa & Bruenn 1993a,b) extended to GR. The other code, *MGFLD-TRANS*, developed by (Bruenn, DeNisco, & Mezzacappa 2000a), couples GR multigroup flux-limited diffusion (MGFLD) to Lagrangian GR hydrodynamics. Both codes give qualitatively similar results for core collapse simulations, and quantitative comparisons are in progress.

Our purpose in this paper is to present results of simulations performed with *MGFLD-TRANS* of the collapse, bounce, and subsequent (~ 1 second) evolution of the cores of massive stars. These simulations will be compared with Newtonian simulations, performed with the Newtonian limit of this same code, in order to assess the effects of general relativity for the evolution of the stellar core, particularly during the critical phase in which the shock stalls and the success or failure of the supernova explosion is thereafter by a competition between the neutrino heating behind the shock and the accretion ram. The code itself will be described in detail in another paper (Bruenn et al. 2000a), but we will give a further very brief description below.

MGFLD-TRANS solves the GR hydrodynamics equations, the GR MGFLD transport equations, and the Einstein equations. A $3 + 1$ formalism using a diagonal gauge is used to advance the equations in time. The metric used is

$$ds^2 = a^2(t, m)c^2 dt^2 - b^2(t, m)dm^2 - r^2(t, m)(d\theta^2 + \sin^2\theta d\phi^2) \quad (1)$$

where m is the total rest mass enclosed by a shell of radius r , and a and b are metric functions. Operator splitting is used to couple the hydrodynamics and transport codes and, very roughly speaking, is implemented by advancing first the matter configuration and metric functions through a time step $t \rightarrow t + \Delta t$ using the GR hydrodynamics (using the neutrino fields at time t), and then advancing the neutrino distribution through the same time step with the GR MGFLD code. The code is capable of performing 1D fully

GR simulations of all phases of stellar core collapse and core collapse supernovae. Because of the sensitivity of the supernova mechanism to the neutrino spectra, we believe it is essential that numerical simulations be performed with *multigroup* neutrino transport. In this way, the neutrino spectrum is computed *ab initio*, rather than assumed, and the critical energy-dependent neutrino interactions can therefore be calculated accurately.

The plan of this paper is as follows: In Section 2 we give a brief account of the current core collapse supernova paradigm in order to set the stage for this work. We then outline in Section 3 our numerical methods and the simulations we perform. Because matter hydrodynamics and neutrino transport are closely coupled during stellar core collapse, we compare Newtonian and GR hydrodynamics in Section 4. This provides a basis for distinguishing between the modifications of neutrino transport that arise “directly” from the GR terms in the transport equations and those that arise from the effects of GR on the hydrodynamics. Neutrino transport is our focus in Section 5, where we investigate the effects of GR by comparing dynamical simulations that use various combinations of Newtonian and GR hydrodynamics and transport. We state our conclusions in Section 6.

2. Supernova Paradigm

To set the stage for this work, we very briefly review the current core collapse supernova paradigm, which is referred to as the “shock reheating mechanism” or “delayed mechanism” (Wilson 1985; Bethe & Wilson 1985). It is based on the original Colgate & White (1966) idea that a core collapse supernova explosion is driven by neutrino energy deposition, but the paradigm has been much modified and refined over the intervening years. All investigators agree with the paradigm’s account of the initial phases of the mechanism, which starts with the destabilization and collapse of the core of a massive star. When the density of the core exceeds nuclear matter density, the homologously collapsing inner

core rebounds and drives a shock into the outer core. This “bounce” shock, which must ultimately explode the star, weakens and stalls between 100 and 200 km. This temporary “demise” of the shock is brought about by the reduction in the postshock pressure due to both the dissociation of nuclei in the material passing through by the shock and the intense outward radiation of neutrinos from the postshock region. The stalled shock becomes an accretion shock, separating the supersonically infalling material at larger radii from the material at smaller radii, which is subsonically settling onto the surface of the proto-neutron star. Within 10’s of milliseconds, the structure of the core becomes quasi-steady-state. Infalling matter encounters the shock and is shock dissociated into free nucleons. As these nucleons continue to flow subsonically inward, they are heated by absorbing a small fraction of the neutrinos that are being radiated from the hot contracting core. As this accreting matter continues to flow inward, neutrino and compressional heating increase its temperature until the cooling rate, which goes as the sixth power of the temperature, exceeds the heating rate. The inflowing matter thereafter cools and ultimately accretes onto the core. An important radius that we will have a number of occasions to refer to is the “gain radius,” at which the heating and cooling rates balance. Above the gain radius, heating by the absorption of neutrinos dominates; below the gain radius, cooling by the emission of neutrinos dominates. (Gain radii can be defined analogously for each neutrino flavor, e.g., the ν_e gain radius is the radius at which ν_e heating and ν_e cooling vanish.)

It is here that the shock reheating mechanism becomes murky, as different groups fail to agree on when, how, or even if the shock is revived. The problem is that simulating this epoch realistically presents many difficulties. Neutrino transport plays a key role, for example, but until now the state of the art in neutrino transport algorithms has been multigroup flux-limited diffusion. In this scheme, the neutrino spectrum is computed as part of the transport solution rather than being assumed, which is very important, but the diffusion and free streaming limits are bridged by interpolation. Unfortunately, this

interpolation encompasses the critical neutrino heating region between the gain radius and the shock. Furthermore, a generic problem with flux-limited diffusion is that it underestimates the isotropy of the neutrino distribution when the transition from large to small neutrino opacities is abrupt, as it is near the neutrinospheres shortly after the formation of the proto-neutron star. [Fortunately, “exact” Boltzmann transport simulations of neutrino transport are becoming available (Mezzacappa & Bruenn 1993c,a,b; Messer et al. 1998; Mezzacappa et al. 2000).] Another difficulty is that the neutrino heating between the gain radius and the shock sets up an unstable entropy gradient that drives convection. This convection, referred to as neutrino-driven convection, may help in reviving the shock, but can only be modeled realistically by multidimensional (preferably 3-dimensional) simulations. It is also likely that fluid instabilities also arise below the neutrinospheres, and these may drive fluid motions which, by advecting entropy and leptons to or from the neutrinospheres, may modify the neutrino transport. It is not clear yet whether these fluid instabilities above and below the neutrinospheres play an essential or a peripheral role in the explosion mechanism. In any case, the radius of the shock is determined by the competition between the thermal and convective pressure generated by neutrino heating, on the one hand, and by the ram pressure of the infalling material on the other. The generation of a successful explosion requires that this radius becomes unstable (Burrows & Goshy 1993) so that quasi-hydrostatic readjustment becomes impossible, i.e., that the neutrino heating be sufficiently rapid in the region between the gain radius and the shock for the thermal and convective pressure to overcome the accretion ram, causing the shock to accelerate outwards. Unfortunately, explosions seem to be marginal at best in many of the detailed numerical simulations, and perhaps in Nature as well; therefore, they depend sensitively on the implementation of the physics and numerics: e.g., the equation of state, neutrino opacities, hydrodynamics, neutrino transport, and general relativity. In particular, realistic simulations of core collapse supernovae must include the effects of GR.

3. Method

To assess the GR effects on the evolution of the core in the context of the above core collapse supernova paradigm, we have performed two sets of simulations, one set initiated from a $15 M_{\odot}$ precollapse model, S15s7b, the other set initiated from a $25 M_{\odot}$ precollapse model, S25s7b. These precollapse models were provided by Woosley (1995), and are described in Woosley & Weaver (1995). The precollapse models S15s7b and S25s7b were chosen to represent small-iron-core and large-iron-core precollapse models, respectively. When core collapse begins, the iron core mass of model S15s7b is $1.278 M_{\odot}$, while that of model S25s7b is $1.770 M_{\odot}$.

The set of simulations initiated from model S15s7b consists of a simulation with Newtonian hydrodynamics and Newtonian transport, referred to as simulation S15s7b_nt, a hybrid simulation with GR hydrodynamics and Newtonian transport, referred to as simulation S15s7b_hyb, and a fully GR simulation, referred to as simulation S15s7b_gr. Likewise, the set of simulations initiated from model S25s7b consists of the same combinations of Newtonian and GR hydrodynamics and transport, and are referred to as S25s7b_nt, S25s7b_hyb, and S25s7b_gr. In each simulation, the model was evolved through core collapse, bounce, and through an 0.8 to 1.0 second interval after bounce. (The simulations beginning with S25s7b with GR hydrodynamics (viz., simulations S25s7b_hyb and S25s7b_gr) resulted in the formation of an event horizon ~ 0.6 seconds after bounce, and had to be terminated.) For the simulations carried out with Newtonian transport (viz., simulations S15s7b_nt, S15s7b_hyb, S25s7b_nt, and S25s7b_hyb), the transport was computed using the Newtonian limit of our fully GR MGFLD code, *MGFLD-TRANS*, described briefly in Section 1. In this limit, the code is essentially as described in Bruenn (1985) and Bruenn & Haxton (1991). We will refer to this transport as “Newtonian MGFLD”, even though, technically, the transport equations in this limit are derived

from the $O(\frac{v}{c})$ Boltzmann equation. For the simulations carried out with GR transport (viz., simulations S15s7b-gr and S25s7b-gr), the neutrino transport was computed with *MGFLD-TRANS* in its fully GR mode.

With the above described simulations, we will compare Newtonian and GR hydrodynamics as they affect such quantities as the locations of the shock, the ν_e and $\bar{\nu}_e$ gain radii, and the infall speed of the matter between the shock and the gain radii (and therefore the time available for a comoving fluid element to be heated by neutrinos). We will also compare Newtonian and GR transport as they affect such quantities as the luminosities and rms energies of each neutrino flavor. Comparisons between the Newtonian and hybrid simulations will highlight the effects on the neutrino transport of the differences between Newtonian and GR hydrodynamics. On the other hand, the hydrodynamics in the hybrid and the fully GR simulations is the same, and comparisons between these simulations will highlight the differences between Newtonian and GR neutrino transport.

In all simulations, the Lattimer-Swesty equation of state (Lattimer & Swesty 1991) was used when the following three conditions were satisfied locally: (1) $n_B > 10^{-8} \text{ fm}^{-3}$ ($\rho > 1.67 \times 10^7 \text{ g cm}^{-3}$), where n_B is the number density of nucleons (free and bound) per cubic Fermi, (2) $T > 0.05 \text{ MeV}$, and (3) the matter was assumed to be in nuclear statistical equilibrium (NSE). The Cooperstein-BCK equation of state (Cooperstein 1985; Baron, Cooperstein, & Kahana 1985) was used when the second and third condition was satisfied, but not the first. For nuclei not in NSE, which comprised the silicon layer, oxygen layer, and other exterior layers until they encountered the shock, the nuclei were treated as an ideal gas (with excited states), and a nine-species nuclear reaction network was used to follow the nuclear transmutations. A zone not in NSE were flashed to NSE if its temperature reached 0.44 MeV (Thielemann, Nomoto, & Hashimoto 1996). Three-flavor GR multigroup flux-limited diffusion, as described in (Bruenn et al. 2000a), was used for the neutrino

transport, with twenty energy zones spanning in geometric progression the neutrino energy range from 4 MeV to 400 MeV. The neutrino microphysics described in Bruenn (1985) and Bruenn & Haxton (1991) was used, as well as the ion screening corrections given by Horowitz (1996), described in detail in Bruenn & Mezzacappa (1997).

4. General Relativistic versus Newtonian Hydrodynamics

The structure of the core during the shock reheating epoch consists of a quasi-stationary accretion shock separating the supersonic infall of mantle material outside the shock from the subsonic inward flow of material between the shock and the surface of the proto-neutron star. This structure is similar to that of a neutron star undergoing hypercritical accretion (i.e., accretion far in excess of the photon Eddington limit), which can occur after the supernova explosion if some of the ejecta falls back onto the neutron star, or if a neutron star spirals into the envelope of a binary companion. Hypercritical accretion has been investigated by Colgate (1971), Zel’dovich, Ivanova, & Nadëzhin (1972), Blondin (1986), Chevalier (1989), Chevalier (1995), and Houck & Chevalier (1991). As emphasized by Houck & Chevalier (1991) and Chevalier (1995), the steady-state position of the shock is determined by the condition that the neutrino radiation, which occurs in a thin layer around the neutron star surface, release the gravitational binding energy gained by the infalling material. The neutrino radiation occurs in a thin layer because of the sensitivity of the neutrino emissivity to the temperature. The dependence is T^9 for the pair process, applicable for the wide range of expected accretion rates ($10^{-8} - 10^4 M_{\odot}/\text{yr}$) after the supernova, and T^6 for electron and positron capture, applicable for the much higher accretion rates (and densities) during the shock reheating epoch.

Houck & Chevalier (1991) studied hypercritical accretion onto a neutron star with GR hydrodynamics and found that the shock radius was reduced by a factor of about two from

the value given by Newtonian hydrodynamics. Their explanation for this GR reduction in shock radius applies to a similar reduction in shock radius found in our simulations of the shock reheating epoch. The explanation begins with the fact that the pressure at the neutron star surface is fixed by the temperature required for neutrinos to radiate away the gravitational binding energy of the infalling material. At a given accretion rate, more binding energy must be radiated away with GR than with Newtonian hydrodynamics because of the more compact core structure and deeper gravitational potential well that results with GR. On the other hand, the high temperature sensitivity of the neutrino emission rates leads to temperatures in the two calculations, and therefore pressures, that do not differ greatly at the emission surface despite the difference in the emission rates. Above the emission surface, however, the stronger effective gravitational field strength in the GR calculation results in a larger pressure gradient. The approximately equal pressures at the neutron star surfaces in the two calculations together with a larger pressure gradient in the GR calculation results, in the latter calculation, in a more compact structure between the neutron star surface and the shock.

Figures 1 and 2 compare the shock radius and the ν_e and $\bar{\nu}_e$ gain radii as a function of time for the postbounce evolution of models S15s7b and S25s7b, respectively, as given by Newtonian and GR hydrodynamics for the same (Newtonian) transport, i.e., simulations S15s7b_nt, S15s7b_hyb, S25s7b_nt, and S25s7b_hyb. We mention again that the ν_e gain radius for the inflowing material is the radius at which cooling by ν_e emission is equal to heating by ν_e absorption. Above the gain radius, ν_e heating dominates; below the gain radius, ν_e cooling dominates. The $\bar{\nu}_e$ gain radius is defined analogously, and, as in the case of the ν_e 's, $\bar{\nu}_e$ heating and cooling dominate above and below the $\bar{\nu}_e$ gain radius, respectively. The energy transfer between neutrinos and matter behind the shock during the postshock evolution considered here is mediated primarily by the charged current reactions

$$\nu_e + n \rightleftharpoons p + e^-, \quad \bar{\nu}_e + p \rightleftharpoons n + e^+. \quad (2)$$

Although μ and τ neutrinos are also emitted by the proto-neutron star at this time, they couple very weakly with the material above the proto-neutron star and, therefore, play a negligible role in matter heating. We omit their gain radii in Figures 1 and 2.

It is seen from the figures that, as in the case of hypercritical accretion onto a fully formed neutron star, the structure above the proto-neutron star during the shock reheating epoch is considerably more compact in the GR simulations than in the Newtonian simulations. The shock radius is reduced by a factor of about 2 after $t_{pb} \sim 0.3$ s for simulation S25s7b_hyb versus simulation S25s7b_nt, and after $t_{pb} = 0.6$ s for simulation S15s7b_hyb versus simulation S15s7b_nt. Throughout most of the postbounce evolution, the distance between the gain radius and the shock is also reduced by a factor of about 2 for the simulations with GR hydrodynamics. This constriction of the heating region exhibited by the simulations with GR hydrodynamics will result in a reduction in the time spent in this region by inwardly moving fluid elements, and therefore, for given neutrino luminosities and rms energies, in a reduction in the net heat acquired by these fluid elements.

In addition to the width of the heating region, the material inflow speed through the heating region affects the net heat acquired by the material, and is modified by the use of GR hydrodynamics. We note first that the material inflow speed through the heating region below the shock is a very shallow function of the radius. This behavior can be understood from the fact that the flow below the shock is subsonic, approximately adiabatic until intense cooling sets in near the neutrinospheres, and has an approximately constant γ , where γ is the adiabatic index. Under these conditions (Chevalier 1989),

$$v \propto r^{(3-2\gamma)/(\gamma-1)}, \quad (3)$$

which follows by integrating the equation of hydrostatic equilibrium and the continuity equation through this region. Now the material below the shock is a mixture of radiation, leptons, and free baryons, with a value of gamma between 1.4 and 1.5. Equation (3) shows that v is indeed a rather shallow function of r for this range of gamma. We can therefore characterize the speed of the material through the heating region by its immediate postshock velocity. Figure 3 compares the postshock velocities as a function of time for simulations S15s7b_nt, S15s7b_hyb, S25s7b_nt, and S25s7b_hyb. It is seen that the postshock velocities given by the simulations with GR hydrodynamics, i.e., simulations S15s7b_hyb and S25s7b_hyb, are substantially larger in magnitude than those given by the simulations with Newtonian hydrodynamics, i.e., simulations S15s7b_nt and S25s7b_nt, the difference being ~ 2 for each model after roughly 0.2 s. The larger postshock velocities in the GR simulations follows from the fact that (a) the immediate preshock velocities in the GR limit are about a factor of 2 larger than those given in Newtonian limit because of the smaller shock radii and the stronger effective gravity in the GR case, and (b) the fact that the ratios of the velocities across the shock are approximately the same for both the Newtonian and GR simulations. The differences between GR and Newtonian hydrodynamics, in particular, the much reduced time that a given fluid element spends between the shock and the gain radius in the GR simulations, may have implications for the development of neutrino-driven convection.

5. General Relativistic versus Newtonian Hydrodynamics and Transport

In this section, we will compare complete dynamic simulations of core collapse with Newtonian hydrodynamics and transport, GR hydrodynamics and Newtonian transport, and GR hydrodynamics and transport.

5.1. Infall and Bounce

We will begin our comparisons with the infall, bounce, and immediate postbounce epochs as computed with Newtonian hydrodynamics and transport, viz., simulations S15s7b_nt and S25s7b_nt, and GR hydrodynamics and transport, viz., simulations S15s7b_gr and S25s7b_gr. Figures 4 – 7 show radius versus time trajectories of Lagrangian surfaces enclosing selected rest masses. Figures 4 and 6 show this for the GR simulations, Figures 5 and 7 show this for the corresponding Newtonian simulations. For both precollapse models, collapse to bounce takes slightly less time in the GR simulations — 0.1829 s for S15s7b_gr versus 0.2013 s for S15s7b_nt, and 0.2723 s for S25s7b_gr versus 0.2895 s for S25s7b_nt. Bounce occurs at a slightly higher density in the GR simulations — 4.23×10^{14} g/cm³ for S15s7b_gr versus 3.20×10^{14} g/cm³ for S15s7b_nt, and 4.15×10^{14} g/cm³ for S25s7b_gr versus 3.34×10^{14} g/cm³ for S25s7b_nt. For both models, the shock propagates slightly farther out in radius in the GR simulations before receding — 172 km for S15s7b_gr versus 155 km for S15s7b_nt, and 231 km for S25s7b_gr versus 226 km for S25s7b_nt. After the secondary quasistatic rise in the shock radius, the shock radius declines considerably more rapidly in the GR simulations than in the corresponding Newtonian simulations.

Figure 8 shows for simulations S15s7b_gr and S15s7b_nt the luminosity as a function of time for ν_e ’s, $\bar{\nu}_e$ ’s, and ν_x ’s. Here ν_x refers to either a ν_μ , $\bar{\nu}_\mu$, ν_τ , or $\bar{\nu}_\tau$. (These have very similar interactions with matter at the energies of importance in core collapse supernovae, and are treated identically in the transport code.) Figure 9 is similar, plotting the ν_e , $\bar{\nu}_e$, and ν_x luminosities as a function of time for simulations S25s7b_gr and S25s7b_nt. The spike in the ν_e luminosity is produced when the shock propagates out through the ν_e -sphere, which at this time is located at a radius of roughly 100 km for all models. The source of the ν_e luminosity spike is (a) the ν_e ’s produced by the rapid electron capture on the free protons released by the shock-dissociated nuclei, and (b) their production near the ν_e -sphere which

results in their rapid escape from the core. The delay in the ν_e -burst for S15s7b_nt relative to S15s7b_gr, and in S25s7b_nt relative to S25s7b_gr, is a consequence of the corresponding delay in the bounce and shock generation in the Newtonian relative to the GR simulations, described above. In the case of simulations S25s7b_gr and S25s7b_nt (Figure 9), there is a small secondary spike in the ν_e and $\bar{\nu}_e$ luminosities that occurs ~ 15 ms after the primary ν_e spike. These spikes are caused by the recollapse of material that occurs ~ 15 ms following bounce, as evident in Figures 6 and 7. The recollapse of material draws in and heats the ν_e and $\bar{\nu}_e$ neutrinospheres, thus hardening the ν_e and $\bar{\nu}_e$ spectra (Figure 11) and increasing their luminosities.

Figure 10 shows for simulations S15s7b_gr and S15s7b_nt the rms energy as a function of time for the ν_e 's, $\bar{\nu}_e$'s, and ν_x 's. Figure 11 is similar, plotting the ν_e , $\bar{\nu}_e$, and ν_x rms energies as a function of time for simulations S25s7b_gr and S25s7b_nt. These figures show that in all the simulations there is a trifurcation of the rms energies of the different neutrino flavors which begins immediately after bounce—the ν_e 's having the smallest rms energy at any given time, and the ν_x 's having the largest. This well known effect is caused by the flavor dependence of the coupling strength of neutrinos with matter, which cause the different neutrino flavors to thermally decouple from the matter at different radii. The ν_e 's and $\bar{\nu}_e$'s thermally couple with matter primarily by the charged current processes (2). For a given neutrino energy, the large neutron to proton ratio in the core endows the matter with higher ν_e opacity than $\bar{\nu}_e$ opacity, and the $\bar{\nu}_e$'s therefore tend to thermally decouple from the matter deeper in the core where it is hotter. The ν_x 's lack any charged current opacity contribution, and they thermally decouple from the matter deepest in the core and thus have the highest rms energies.

A feature in these plots that appears in all the simulations is the prominent spike in the rms energy of the ν_x 's at bounce. The luminosities of the ν_x 's at this time are still small, so

the overall number of ν_x 's affected is small. The spike in the rms energy has its origin in the compression of the ν_x 's by the shock immediately before it propagates through the ν_x -sphere, and is numerical artifact of the pseudoviscous terms in the numerical hydrodynamics which enable the hydrodynamics code to track shock waves automatically, but which spread the shock compression-front over several radial zones. This numerical artifact arises from the fact that, unlike the ν_e 's and $\bar{\nu}_e$'s, the ν_x -opacity is dominated by isoenergetic scattering on nucleons and nuclei. Much weaker are the processes that thermally equilibrate the ν_x 's with matter, i.e., nucleon bremsstrahlung (not included in these simulations), neutrino-electron scattering, and ν_x - $\bar{\nu}_x$ pair annihilation. Therefore, the ν_x -thermalization-sphere, defined as having the radius at which the ν_x 's are last thermally equilibrated with the matter, lies considerably deeper in the core than the ν_x -sphere, defined as having the radius at which the ν_x 's decouple from the matter completely. During the brief time that the supernova shock generated from core bounce propagates outward through the region between the ν_x -thermalization-sphere and the ν_x -sphere, the artificially large width of the pseudoviscous-spread shock compression-front exceeds the ν_x -scattering mean-free-paths, and the ν_x 's are therefore compressed along with the matter and boosted up in energy. The ν_x -spectrum, which normally reflects the conditions at the ν_x -thermalization-sphere, is thus momentarily and unphysically hardened by this shock-compression.

5.2. Shock Reheating

Figure 12 shows a comparison of the ν_e luminosity as a function of time during the shock reheating epoch for simulations S15s7b_nt, S15s7b_hyb, and S15s7b_gr. Figures 13 and 14 are similar to Figure 12 and show, respectively, a comparison of the $\bar{\nu}_e$ luminosity and the ν_x luminosity for these simulations. Figures 15, 16, and 17 show, respectively, a comparison of the ν_e , $\bar{\nu}_e$, and ν_x luminosity as a function of time during the shock reheating

epoch for the simulations S25s7b_nt, S25s7b_hyb, and S25s7b_gr. Figures 15 and 16 show that the ν_e and $\bar{\nu}_e$ luminosities for all simulations of model S25s7b exhibit an abrupt decline beginning at about 0.42 s after bounce. This occurs when the interface between the silicon and oxygen shells passes through the neutrinospheres. There is a considerable jump in entropy and a corresponding drop in density at this interface, and the passage of this interface through the neutrinospheres reduces the mass accretion rate there by almost a factor of three. This substantially reduces the ν_e and $\bar{\nu}_e$ accretion luminosities, and accounts for the above mentioned drop in their overall luminosities. The ν_x luminosity arises deeper in the core, has very little contribution from the accreting matter, and is therefore unaffected by the drop in the mass accretion rate.

Figures 18, 19, and 20 show, respectively, a comparison of the ν_e , $\bar{\nu}_e$, and ν_x rms energy as a function of time from bounce for the simulations S15s7b_nt, S15s7b_hyb, and S15s7b_gr. Figures 21, 22, and 23 do the same for the simulations S25s7b_nt, S25s7b_hyb, and S25s7b_gr. The neutrino luminosities and the rms energies exhibit a trend that is common to all neutrino flavors for both models S15s7b and S25s7b. During the shock reheating phase, the luminosity and rms energy of any neutrino flavor increase when switching from Newtonian to GR hydrodynamics, and decrease when switching from Newtonian to GR transport. The increase in the neutrino luminosity and rms energy in switching from Newtonian to GR hydrodynamics can be understood by recalling that GR hydrodynamics produces a more compact core structure, as discussed in Section 4. This results in hotter neutrinospheres at smaller radii. For example, in simulation S15s7b_nt, at 0.4 s after bounce, the ν_e -sphere has a radius and temperature of 37.7 km and 3.89 MeV, respectively. The corresponding values for radius and temperature in simulation S15s7b_hyb are 29.0 km and 4.80 MeV, respectively. At the same postbounce time, the $\bar{\nu}_e$ -sphere has a radius and temperature of 35.5 km and 4.15 MeV, respectively, in simulation S15s7b_nt, compared to a radius and temperature of 27.0 km and 4.92 MeV, respectively, in

simulation S15s7b_hyb. Moreover, at this time, the ν_x -thermalization-sphere has a radius and temperature of 25.8 km and 6.53 MeV, respectively, in simulation S15s7b_nt compared to a radius and temperature of 24.28 km and 7.66 MeV, respectively, in S15s7b_hyb.

The decrease in the luminosity and rms energy of all neutrino flavors when switching from Newtonian to GR transport is primarily a consequence of (a) gravitational redshift, as the neutrinos propagate out to large distances, and (b) the difference between the rate of proper time at the respective neutrinospheres and at large radii. The gravitational redshift occurs as a neutrino propagates from its neutrinosphere to a large radius and affects both the neutrino luminosity and rms energy. The difference between the rates of proper time causes an additional reduction in the neutrino luminosity (by the same factor as the gravitational redshift), as it causes an observer at a large radius to see a reduced rate of photon emission from the neutrinosphere.

The radii and temperatures of the various ν -spheres are similar for simulations S15s7b_hyb and S15s7b_gr at corresponding times after bounce. The same is true for simulations S25s7b_hyb and S25s7b_gr. They differ from the radii and temperatures given by the corresponding Newtonian simulations, S15s7b_nt and S25s7b_nt, mainly by the tendency, discussed above, of the GR hydrodynamics to produce a more compact and hotter core structure. Therefore, the main effect on the radii and temperatures of the various ν -spheres occurs when switching from Newtonian to GR hydrodynamics. However, there are some other rather small effects on the properties of the ν -spheres that occur when switching from the hybrid to the fully GR simulations. For example, as the neutrinos gradually decouple from the matter, they propagate outward with increasingly long mean free paths. In the simulations with GR transport, they consequently suffer some gravitational redshifting between successive interactions with the matter before they completely decouple. This slightly lowers their rms energies, reduces their interaction cross

sections, and causes them to decouple from the matter at a slightly smaller radius. The net effect is a slight reduction (about 0.2 km) in the radii of the neutrinospheres. These small effects will be discussed in Bruenn et al. (2000a), along with a detailed description of the GR transport code.

6. Discussion and Conclusions

We have developed a general relativistic MGFLD neutrino transport code, coupled it to Lagrangian GR hydrodynamics, and used it to simulate core collapse supernovae. Beginning with several precollapse models, we have performed purely Newtonian simulations, hybrid simulations using general relativistic hydrodynamics and Newtonian MGFLD neutrino transport, and fully general relativistic simulations. We have shown that the effect of general relativistic hydrodynamics, versus Newtonian hydrodynamics, is to make substantially more compact the structure of the core up to the stagnated shock: the shock radius is reduced by a factor of 2 for postbounce times exceeding 300 ms for model S25s7b and 600 ms for model S15s7b. Moreover, the inflow speed of the material behind the shock is also increased by about a factor of 2 throughout most of the postbounce evolution in these models.

We have also compared the ν_e , $\bar{\nu}_e$, and ν_x luminosities and rms energies for the same three sets of simulations. We find that switching from Newtonian to GR *hydrodynamics* increases the luminosity and rms energy of all neutrino flavors during the shock reheating epoch. This arises because of the more compact core structures that develop with GR hydrodynamics, which yields ν -spheres at smaller radii and higher temperatures. The higher ν -sphere temperatures increase the luminosities and rms energies of all three neutrino flavors. The smaller radii reduce their luminosities, but not enough to offset the luminosity increase due to the higher temperatures. Switching from Newtonian to GR *transport* reduces the luminosities and rms energies of all three neutrino flavors during the shock

reheating epoch because of the gravitational redshift of the neutrinos as they propagate out to large radii and because of the difference between the rate of proper time at the various ν -spheres compared with the rate of proper time at larger radii. With one exception (the rms ν_x energies for model S15s7b), the reduction in neutrino luminosities and rms energies when switching from Newtonian to GR *transport* does not fully compensate for the increase in these quantities when switching from Newtonian to GR *hydrodynamics*. Therefore, the net effect in switching from a fully Newtonian to a fully GR simulation in most cases is an increase in both the luminosities and rms energies of neutrinos of all flavors during the shock reheating epoch.

The results described in this paper show that GR effects make substantial changes in both the structure of the postcollapse core and the neutrino emission (luminosities and spectra) at this epoch. Therefore, it is important that simulations focused on the supernova mechanism, observables such as the neutrino signatures in underground neutrino observatories, and the nucleosynthesis occurring in the neutrino-driven wind immediately following a supernova explosion, be carried out in the fully GR limit.

SWB and KRD are supported at Florida Atlantic University in part by NSF grant AST-9618423 and NASA grant NAG5-3903. AM is supported at the Oak Ridge National Laboratory, managed by UT-Battelle, LLC, for the U.S. Department of Energy under contract DE-AC05-00OR22725. Some of the simulations presented here were performed on the Multidisciplinary Research Computing Facility (MDRCF) at the College of Science at Florida Atlantic University, funded in part by FAU and the NSF.

REFERENCES

- Arnett, W. D. 1996, *Supernovae and Nucleosynthesis, An Investigation of the History of Matter, from the Big Bang to the Present* (Princeton University Press)
- Baron, E., Bethe, H. A., Brown, G. E., Cooperstein, J., & Kahana, S. 1987, *Physical Review Letters*, 59, 736
- Baron, E., Cooperstein, J., & Kahana, S. 1985, *Physical Review Letters*, 55, 126
- Baron, E., Myra, E. S., Cooperstein, J., & van den Horn, L. J. 1989, *Astrophysical Journal*, 339, 978
- Bethe, H. H. & Wilson, J. R. 1985, *Astrophysical Journal*, 295, 14
- Bionta, R., Blewitt, G., Bratton, C. B., Casper, D., Ciocio, A., R., C., Cortez, B., Crouch, M., Dye, S. T., Errede, S., Foster, G. W., Gajewski, W., Ganezer, K. S., Goldhaber, M., Haines, T. J., Jones, T. W., Kielczewska, D., Kropp, W. R., Learned, J. G., LaSecco, J. M., Mathews, J., Miller, R., Mudan, M. S., Park, H. S., Price, L. R., Reines, F., Schultz, J., Seidel, S., Shumard, E., Sinclair, D., Sobel, H. W., Stone, J. L., Sulak, L. R., Svoboda, R., Thornton, G., van der Velde, J. C., & Wuest, C. 1987, *Physical Review Letters*, 58, 1494
- Blondin, J. M. 1986, *Astrophysical Journal*, 308, 755
- Bowers, R. L. & Wilson, J. R. 1982, *Astrophysical Journal Supplement*, 50, 115
- Bruenn, S. W. 1985, *Astrophysical Journal Supplement*, 58, 771
- Bruenn, S. W. & DeNisco, K. R. 2000, *Astrophysical Journal*, in press
- Bruenn, S. W., DeNisco, K. R., & Mezzacappa, A. 2000a, *Astrophysical Journal*, in press

- Bruenn, S. W., Freund, T., & Mezzacappa, A. 2000b, *Astrophysical Journal*, in preparation
- Bruenn, S. W. & Haxton, W. C. 1991, *Astrophysical Journal*, 376, 678
- Bruenn, S. W. & Mezzacappa, A. 1997, *Physical Review D*, 56, 7529
- . 2000, *Astrophysical Journal*, in preparation
- Burrows, A. & Goshy, J. 1993, *Astrophysical Journal Letters*, 416, L75
- Burrows, A., Hayes, J., & Fryxell, B. A. 1995, *Astrophysical Journal*, 450, 830
- Burrows, A. & Sawyer, R. 1998, *Physical Review C*, 58, 554
- Chevalier, R. A. 1989, *Astrophysical Journal*, 346, 847
- . 1995, *Physics Reports*, 256, 95
- Colgate, S. A. 1971, *Astrophysical Journal*, 163, 221
- Colgate, S. A. & White, R. H. 1966, *Astrophysical Journal*, 143, 626
- Cooperstein, J. 1985, *Nuclear Physics*, A438, 722
- Cooperstein, J., van den Horn, J. J., & A., B. E. 1986, *Astrophysical Journal*, 309, 653
- Duncan, R. C., Shapiro, S. L., & Wasserman, I. 1986, *Astrophysical Journal*, 309, 141
- Ewan, G. T. 1992, *Nuclear Instrumentation Methods A*, 314, 373
- . 1996, *Hyperfine Interactions*, 103, 199
- Fryer, C. L. 1999, *Astrophysical Journal*, 522, 413
- Fryer, C. L., Herant, M., Benz, W., & Colgate, S. A. 1999, *Astrophysical Journal*, 516, 892
- Fuller, G. M. & Meyer, B. S. 1995, *Astrophysical Journal*, 453, 792

- Fuller, G. M. & Qian, Y.-Z. 1996, Nuclear Physics, A606, 167
- Haxton, W. C., Langanke, K., Qian, Y.-Z., & Vogel, P. 1997, Physical Review Letters, 78, 2694
- Herant, M., Benz, W., & Colgate, S. A. 1992, Astrophysical Journal, 395, 642
- Herant, M., Benz, W., Hix, W. R., Fryer, C. L., & Colgate, S. A. 1994, Astrophysical Journal, 435, 339
- Hirata, K., Kajita, T., Koshiba, M., Nakahata, M., Oyama, Y., Sato, N., Suzuki, A., Takita, M., Totsuka, Y., Kifune, T., Suda, T., Takahashi, K., Tanimori, T., Miyano, K., Yamada, M., Beier, E. W., Feldscher, L. B., Kim, S. B., Mann, A. K., Newcomer, F. M., Van Berg, R., Zhang, W., & Cortez, B. G. 1987, Physical Review Letters, 58, 1489
- Hoffman, R. D., Woosley, S. E., & Qian, Y.-Z. 1997, Astrophysical Journal, 482, 951
- Hoffman, R. D., Woosley, S. E., Weaver, T.-A., Rauscher, T., & Thielemann, F.-K. 1999, Astrophysical Journal, 521, 735
- Horowitz, C. 1996, astro-ph/9603138
- Houck, J. C. & Chevalier, R. A. 1991, Astrophysical Journal, 376, 234
- Howard, W. M., Gorierly, S., Rayet, M., & Arnould, M. 1993, Astrophysical Journal, 417, 713
- Janka, H.-T. 1993, in Conference Proceedings Volume 40, Frontiers Objects in Astrophysics and Particle Physics, ed. F. Giovannelli & S. I. F. Mannocchi (Bologna), 345
- Janka, H.-T., Keil, G., Raffelt, G., & Seckel, D. 1996, Physical Review Letters, 76, 2621

- Janka, H.-T. & Müller, E. 1996a, *Astrophysical Journal Letters*, 448, L109
- . 1996b, *Astronomy and Astrophysics*, 306, 167
- Käppeler, F., Thielemann, F.-K., & Wiescher, M. 1998, *Annual Review of Nuclear and Particle Science*, 48, 175
- Keil, W., Janka, H.-T., & Raffelt, G. 1995, *Physical Review D*, 51, 6635
- Lichtenstadt, I., Khokhlov, A. M., & Wheeler, J. C. 1999, *Astrophysical Journal*
- Liebendörfer, M. 2000, PhD thesis, Universität Basel, Switzerland
- Liebendörfer, M., Mezzacappa, A., & Thielemann, F.-K. 2000, *Astrophysical Journal*, submitted
- Lindquist, R. W. 1966, *Annals of Physics*, 37, 487
- May, M. M. & White, R. H. 1966, *Physical Review*, 141, 1232
- Mayle, R. W. 1985, PhD thesis, University of California, Berkeley
- Mayle, R. W. & Wilson, J. R. 1988, *Astrophysical Journal*, 334, 909
- Mayle, R. W. & Wilson, J. R. 1991, in *Supernovae*, ed. S. E. Woosley (New York: Springer), 333
- McLaughlin, G. C. & Fuller, G. M. 1995, *Astrophysical Journal*, 455, 202
- . 1996, *Astrophysical Journal Letters*, 464, L143
- McLaughlin, G. C., Fuller, G. M., & R., W. J. 1996, *Astrophysical Journal*, 472, 440
- Messer, O. E. B., Mezzacappa, A., Bruenn, S. W., & Guidry, M. W. 1998, *Astrophysical Journal*, 507, 353

- Meyer, B. S. 1993, *Physics Reports*, 227, 257
- . 1994, *Annual Reviews of Astronomy and Astrophysics*, 32, 153
- . 1995, *Astrophysical Journal Letters*, 449, L55
- Meyer, B. S. & Brown, J. S. 1997, *Astrophysical Journal Supplement*, 112, 199
- Meyer, B. S., Mathews, G. J., Howard, W. M., Woosley, S. E., & Hoffman, R. D. 1992, *Astrophysical Journal*, 399, 656
- Meyer, B. S., McLaughlin, G. C., & Fuller, G. M. 1998, *Phys. Rev. C*, 58, 3696
- Mezzacappa, A. & Bruenn, S. W. 1993a, *Astrophysical Journal*, 405, 669
- . 1993b, *Astrophysical Journal*, 410, 740
- . 1993c, *Astrophysical Journal*, 405, 637
- Mezzacappa, A., Calder, A. C., Bruenn, S. W., Blondin, J. M., Guidry, M. W., Strayer, M. R., & Umar, A. S. 1998a, *Astrophysical Journal*, 493, 848
- . 1998b, *Astrophysical Journal*, 495, 911
- Mezzacappa, A., Liebendörfer, M., Messer, O. E. B., Hix, R. M., Thielemann, F.-T., & Bruenn, S. W. 2000, *Physical Review Letters*, submitted
- Mezzacappa, A. & Matzner, R. A. 1989, *Astrophysical Journal*, 343, 853
- Miller, D. S., Wilson, J. R., & Mayle, R. W. 1993, *Astrophysical Journal*, 415, 278
- Misner, C. W. & Sharp, D. H. 1965, *Physics Letters*, 15, 279
- Moorhead, M. E. 1997, in *Neutrino Astrophysics*, ed. M. e. a. Altmann (Ringberg, Germany)
- Myra, E. S. & Bludman, S. A. 1989, *Astrophysical Journal*, 340, 384

- Nakamura, T., Kajita, T., Nakahata, M., & Suzuki, A. 1994a, in *Physics and Astrophysics of Neutrinos*, ed. M. Fukugita & A. Suzuki (Tokyo: Springer), 249
- Nakamura, T., Kajita, T., Nakahata, M., & Suzuki, A. 1994b, *Progress in Theoretical Physics*, 100, 921
- Otsuki, K., Tagoshi, H., Kajino, T., & Wanajo, S.-Y. 2000, *Astrophysical Journal*, 533, 424
- Qian, Y.-Z., Haxton, W. C., Langanke, K., & Vogel, P. 1997, *Physical Review*, C55, 1532
- Qian, Y.-Z. & Woosley, S. E. 1996, *Astrophysical Journal*, 471, 331
- Raffelt, G. & Seckel, D. 1991, *Physical Review Letters*, 67, 2605
- Schinder, P. J. 1988, *Physical Review D*, 38, 1673
- Schwartz, R. A. 1967, *Annals of Physics*, 43, 42
- Sigl, G. 1997, *Physical Review D*, 56, 3179
- Sur, B. 1994, in *Intersections Between Particle and Nuclear Physics*, ed. S. J. Seestrom (New York: American Institute of Physics), 112
- Swesty, F. D., Lattimer, J. M., & Myra, E. M. 1994, *Astrophysical Journal*, 425, 195
- Takahashi, K., Witt, J., & Janka, H.-T. 1994, *Astronomy and Astrophysics*, 286, 857
- Thielemann, F.-K., Nomoto, K., & Hashimoto, M. 1996, *Astrophysical Journal*, 460, 408
- Timmes, F. X., Woosley, S. E., & Weaver, T. A. 1995, *Astrophysical Journal Supplement*, 98, 617
- Totsuka, Y. 1992, *Reports on Progress of Physics*, 55, 337
- Van Riper, K. A. 1978, *Astrophysical Journal*, 221, 304

- . 1979, *Astrophysical Journal*, 232, 558
- . 1982, *Astrophysical Journal*, 257, 793
- . 1988, *Astrophysical Journal*, 326, 235
- Van Riper, K. A. & Arnett, W. D. 1978, *Astrophysical Journal Letters*, 225, L129
- Van Riper, K. A. & Lattimer, J. M. 1981, *Astrophysical Journal*, 249, 270
- Weaver, T. A. & Woosley, S. E. 1980, *Annals of the New York Academy of Science*, 336, 335
- Wilson, J. R. 1971, *Astrophysical Journal*, 163, 209
- Wilson, J. R. 1985, in *Numerical Astrophysics*, ed. J. M. Centrella, J. M. LeBlanc, & R. L. Bowers (Boston: Jones and Bartlett), 422–434
- Wilson, J. R. & Mayle, R. W. 1993, *Physics Reports*, 227, 97
- Witte, J., Janka, H.-T., & Takahashi, K. 1994, *Astronomy and Astrophysics*, 286, 841
- Woosley, S. E. 1988, *Astrophysical Journal*, 330, 218
- . 1995, Private Communication
- Woosley, S. E. & Hoffman, R. D. 1992, *Astrophysical Journal*, 395, 202
- Woosley, S. E. & Weaver, T. A. 1995, *Astrophysical Journal Supplement*, 101, 181
- Woosley, S. E., Wilson, J. R., Mathews, G. J., Hoffman, R. D., & Meyer, B. S. 1994, *Astrophysical Journal*, 433, 229
- Zel’dovich, Y. B., Ivanova, L. N., & Nadëzhin, D. K. 1972, *Soviet Astronomy–AJ*, 16, 209

Fig. 1.— Shock and gain radii as functions of time from bounce for simulations S15s7b_nt and S15s7b_hyb. The dashed lines refer to the simulation S15s7b_nt (Newtonian hydrodynamics), the solid lines refer to the simulation S15s7b_hyb (GR hydrodynamics). Both simulations utilize Newtonian transport.

Fig. 2.— Same quantities shown in Figure 1, but for simulations S25s7b_nt and S25s7b_hyb..

Fig. 3.— Postshock velocity as a function of time for simulations S15s7b_nt, S15s7b_hyb, S25s7b_nt, and S25s7b_hyb. The dashed lines refer to the simulations with Newtonian hydrodynamics (S15s7b_nt and S25s7b_nt), and the solid lines refer to the simulations with GR hydrodynamics (S15s7b_hyb and S25s7b_hyb). All simulations utilize Newtonian transport.

Fig. 4.— Radii as a function of time of spherical shells at selected rest masses for the fully GR simulation, S15s7b_gr, for the first 0.69 s.

Fig. 5.— Radii as a function of time of spherical shells at selected rest masses for the Newtonian simulation, S15s7b_nt, for the first 0.65 s.

Fig. 6.— Radii as a function of time of spherical shells at selected rest masses for the fully GR simulation, S25s7b_gr, for the first 0.55 s.

Fig. 7.— Radii as a function of time of spherical shells at selected rest masses for the fully Newtonian simulation, S25s7b_nt, for the first 0.56 s.

Fig. 8.— Neutrino luminosities for each neutrino flavor as a function of time for simulations S15s7b_gr (fully GR) and S15s7b_nt (Newtonian) for the first 0.7 s. The ν_μ ’s, ν_τ ’s and their antiparticles are treated identically in the code, and the luminosity of each is shown by the curves denoted by ν_x . Solid curves refer to simulation S15s7b_gr and are denoted by “(GR)”; dashed curves refer to simulation S15s7b_nt and are denoted by “(NT)”.

Fig. 9.— The same quantities shown in Figure 8 but for simulations S25s7b_nt and S25s7b_gr for the first 0.55 s.

Fig. 10.— Neutrino rms energies for each neutrino flavor as a function of time for simulations S15s7b_gr (fully GR) and S15s7b_nt (Newtonian) for the first 0.7 s. The ν_μ ’s, ν_τ ’s and their antiparticles are treated identically in the code, and the rms energies of each is shown by the curves denoted by ν_x . Solid curves refer to simulation S15s7b_gr and are denoted by “(GR)”; dashed curves refer to simulation S15s7b_nt and are denoted by “(NT)”.

Fig. 11.— The same quantities shown in Figure 10, but for simulations S25s7b_nt and S25s7b_gr for the first 0.55 s.

Fig. 12.— Comparison of the ν_e luminosities as a function of time from bounce for simulation S15s7b_nt (dotted line), simulation S15s7b_hyb (dashed line), and simulation S15s7b_gr (solid line).

Fig. 13.— Comparison of the $\bar{\nu}_e$ luminosities as a function of time from bounce for simulation S15s7b_nt (dotted line), simulation S15s7b_hyb (dashed line), and simulation S15s7b_gr (solid line).

Fig. 14.— Comparison of the $\bar{\nu}_x$ luminosities as a function of time from bounce for simulation S15s7b_nt (dotted line), simulation S15s7b_hyb (dashed line), and simulation S15s7b_gr (solid line). Here ν_x refers to either the ν_μ ’s, ν_τ ’s, or their respective antiparticles.

Fig. 15.— Comparison of the ν_e luminosities as a function of time from bounce for simulation S25s7b_nt (dotted line), simulation S25s7b_hyb (dashed line), and simulation S25s7b_gr (solid line).

Fig. 16.— Comparison of the $\bar{\nu}_e$ luminosities as a function of time from bounce for simulation S25s7b_nt (dotted line), simulation S25s7b_hyb (dashed line), and simulation S25s7b_gr (solid line).

Fig. 17.— Comparison of the $\bar{\nu}_x$ luminosities as a function of time from bounce for simulation S25s7b_nt (dotted line), simulation S25s7b_hyb (dashed line), and simulation S25s7b_gr (solid line). Here ν_x refers to either the ν_μ 's, ν_τ 's, or their respective antiparticles.

Fig. 18.— Comparison of the ν_e rms energies as a function of time from bounce for simulation S15s7b_nt (dotted line), simulation S15s7b_hyb (dashed line), and simulation S15s7b_gr (solid line).

Fig. 19.— Comparison of the $\bar{\nu}_e$ rms energies as a function of time from bounce for simulation S15s7b_nt (dotted line), simulation S15s7b_hyb (dashed line), and simulation S15s7b_gr (solid line).

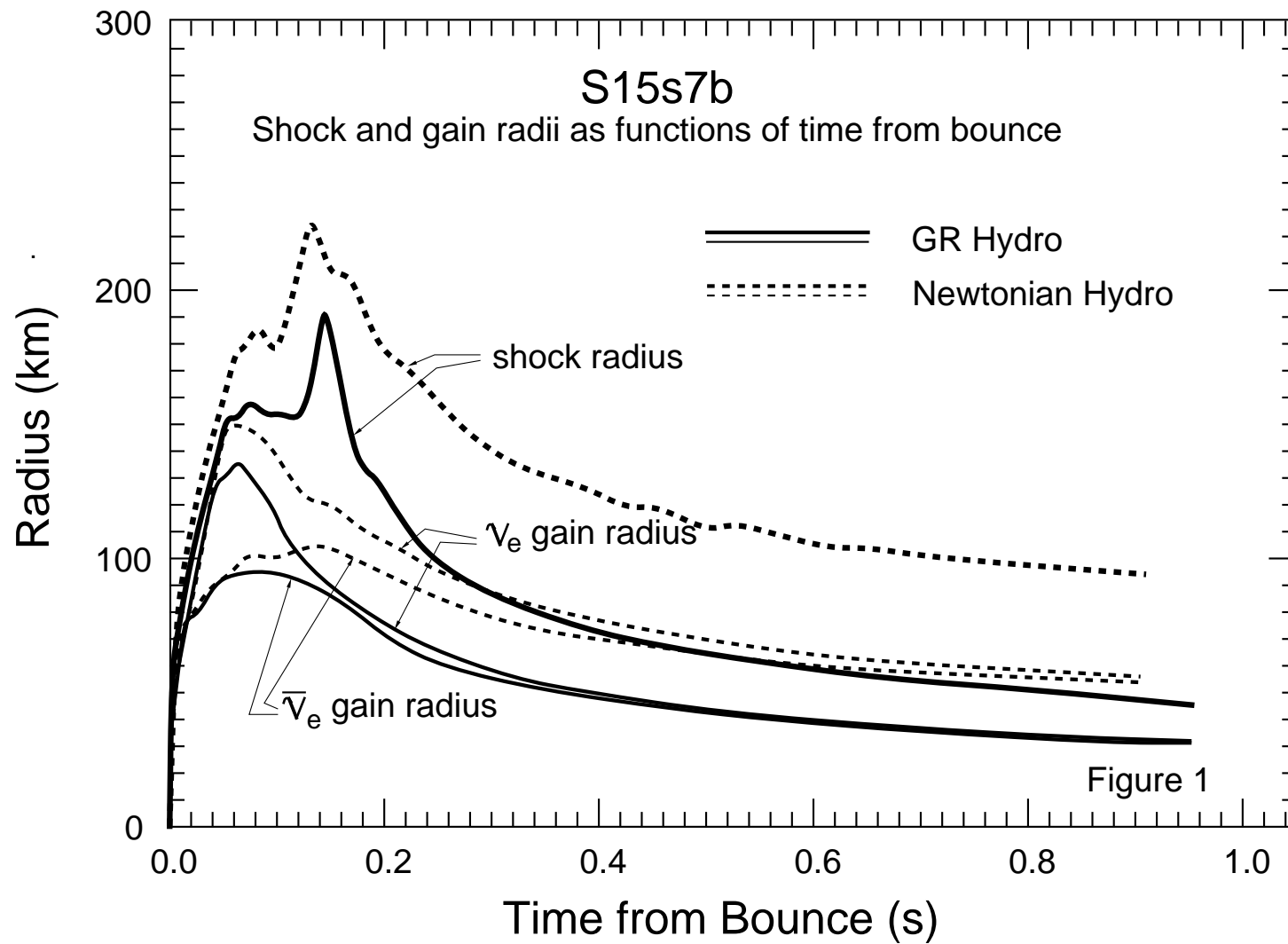
Fig. 20.— Comparison of the $\bar{\nu}_x$ rms energies as a function of time from bounce for simulation S15s7b_nt (dotted line), simulation S15s7b_hyb (dashed line), and simulation S15s7b_gr (solid line). Here ν_x refers to either the ν_μ 's, ν_τ 's, or their respective antiparticles.

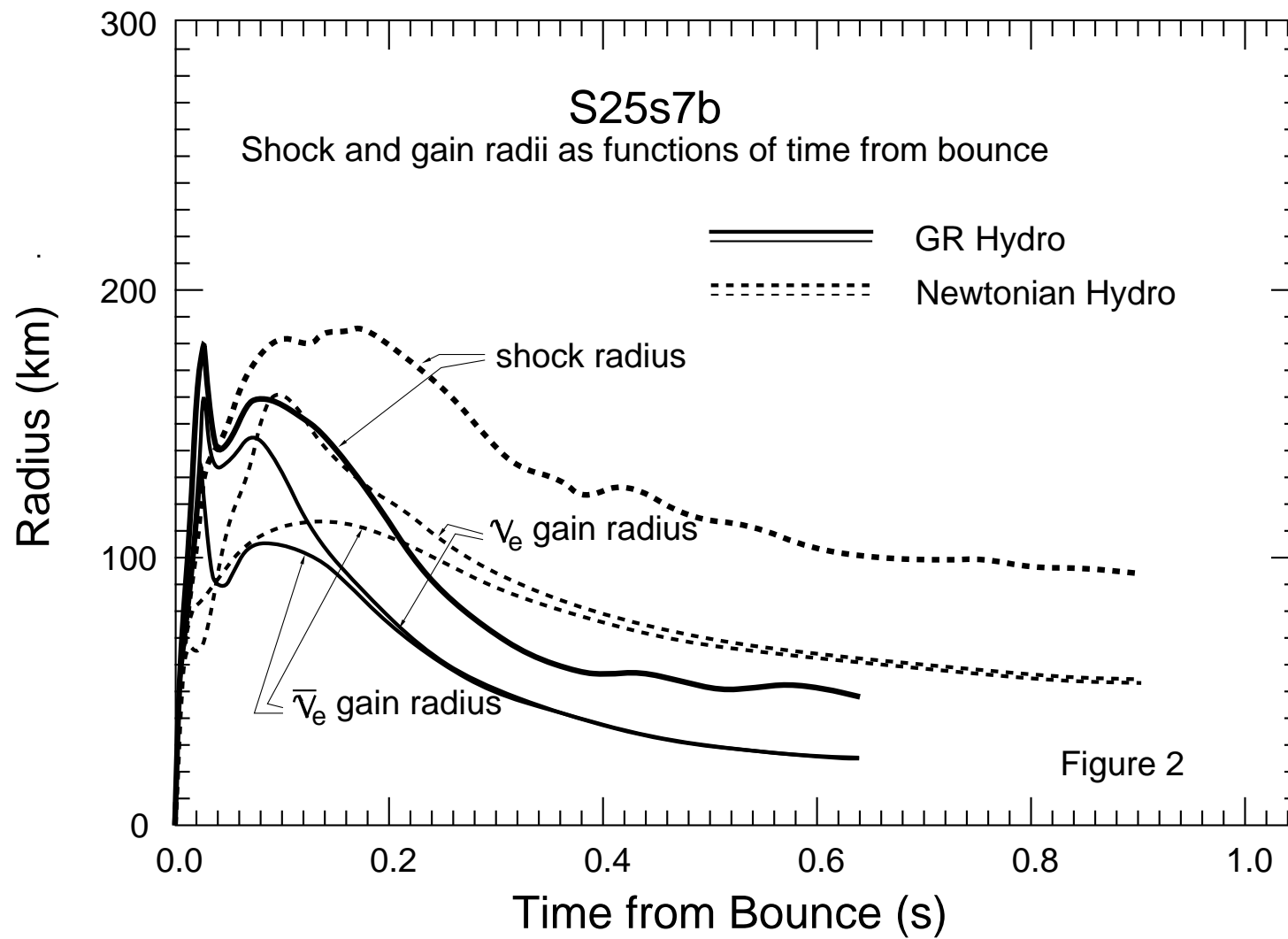
Fig. 21.— Comparison of the ν_e rms energies as a function of time from bounce for simulation S25s7b_nt (dotted line), simulation S25s7b_hyb (dashed line), and simulation S25s7b_gr (solid line).

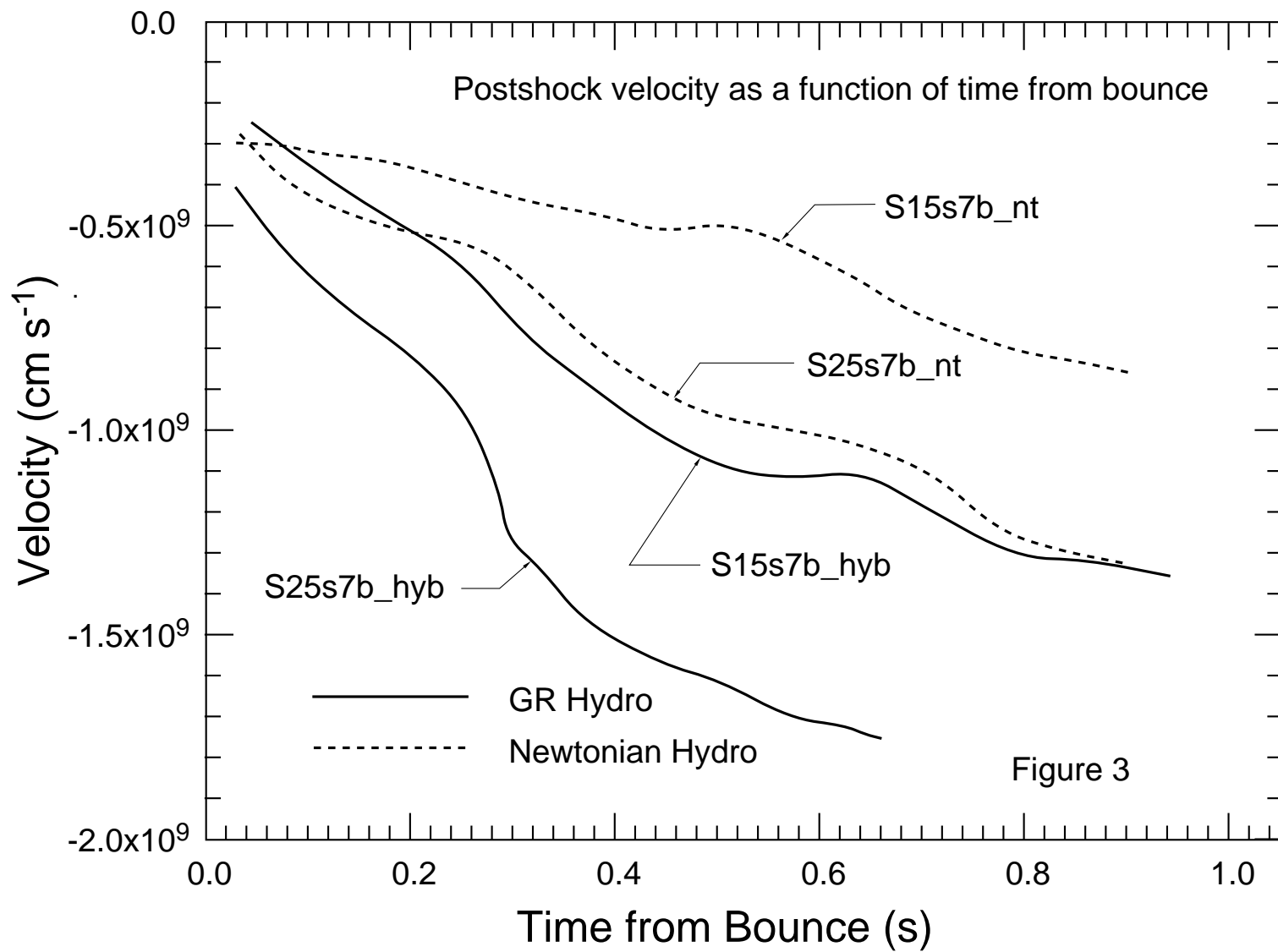
Fig. 22.— Comparison of the $\bar{\nu}_e$ rms energies as a function of time from bounce for simulation

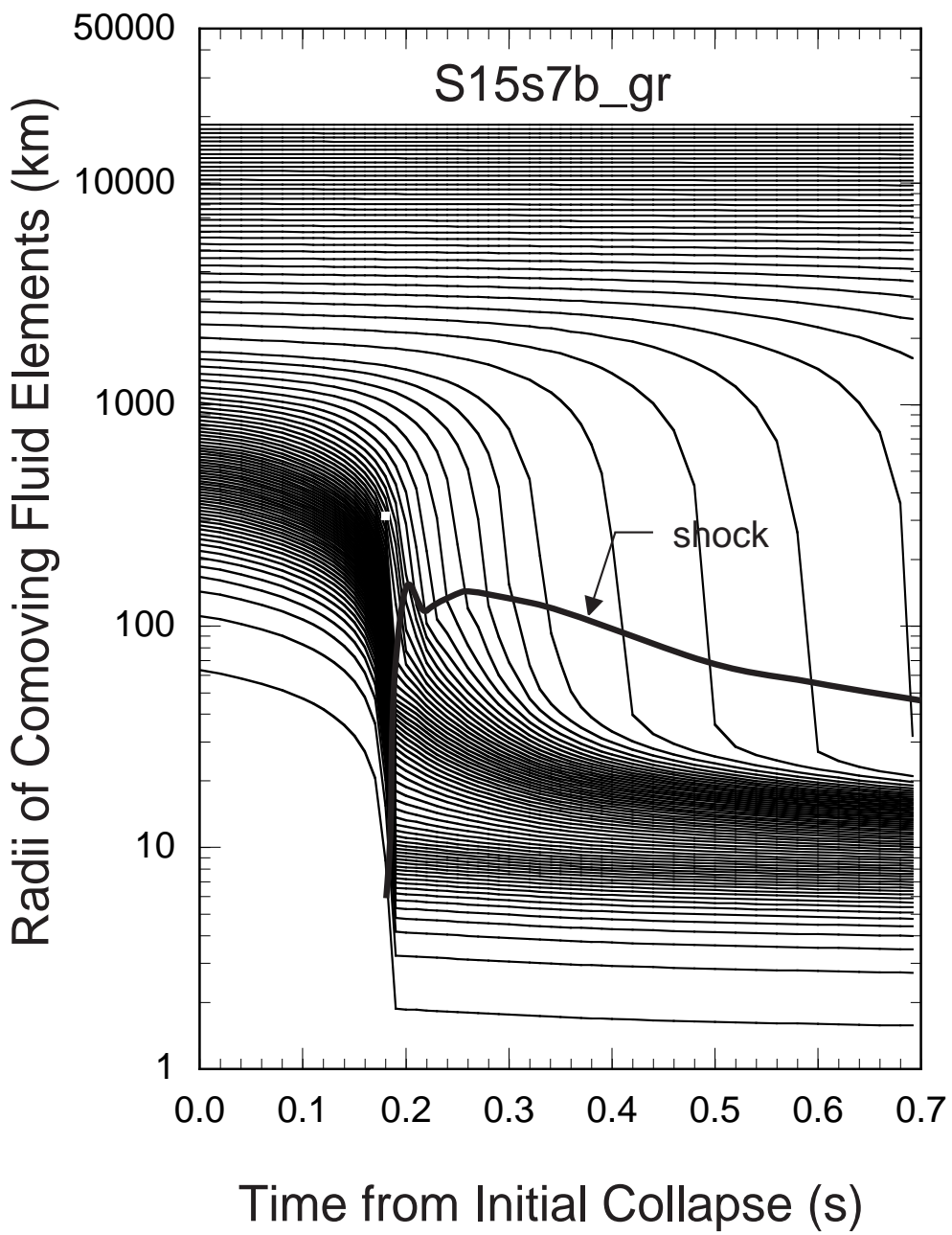
S25s7b_nt (dotted line), simulation S25s7b_hyb (dashed line), and simulation S25s7b_gr (solid line).

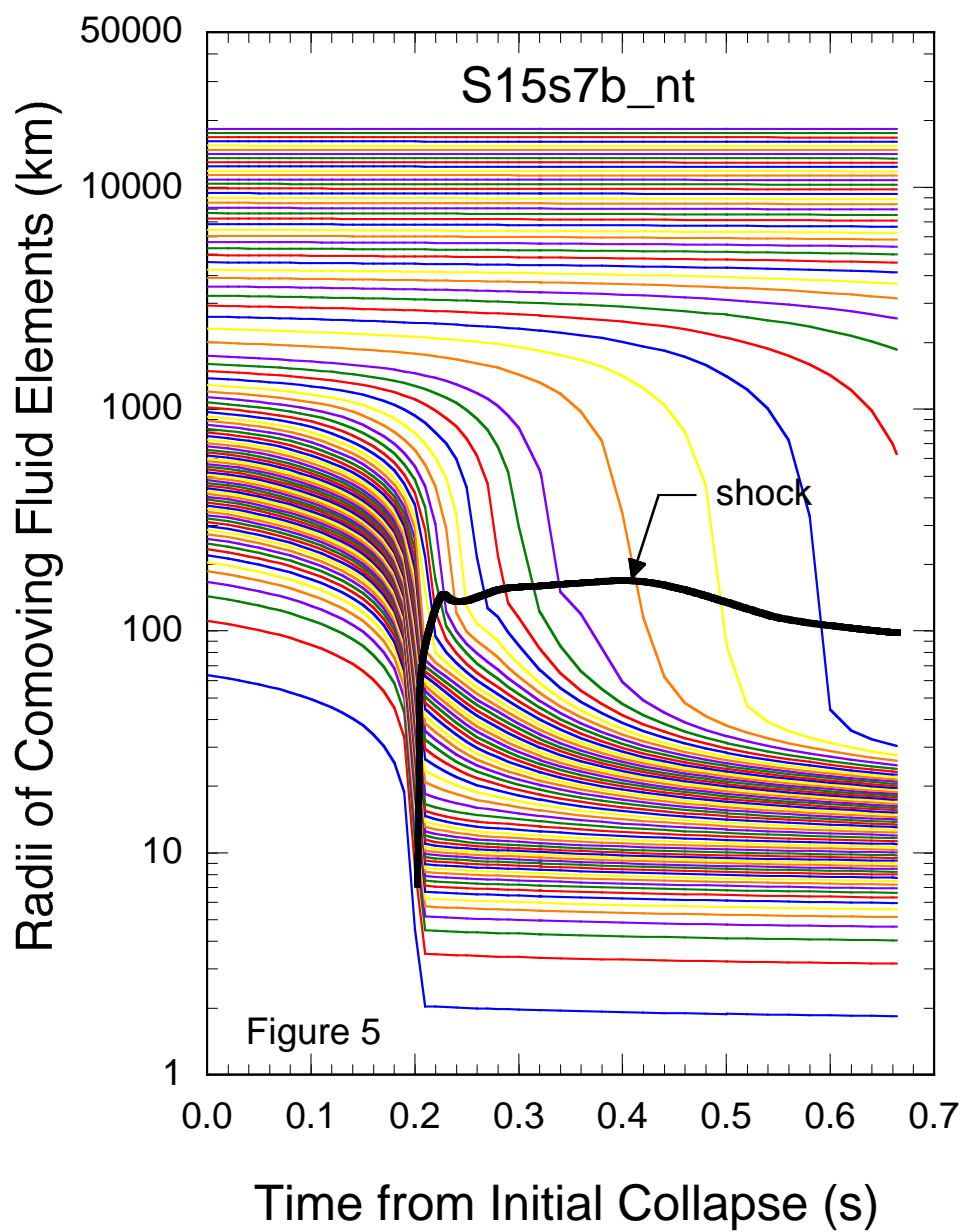
Fig. 23.— Comparison of the $\bar{\nu}_x$ rms energies as a function of time from bounce for simulation S25s7b_nt (dotted line), simulation S25s7b_hyb (dashed line), and simulation S25s7b_gr (solid line). Here ν_x refers to either the ν_μ 's, ν_τ 's, or their respective antiparticles.

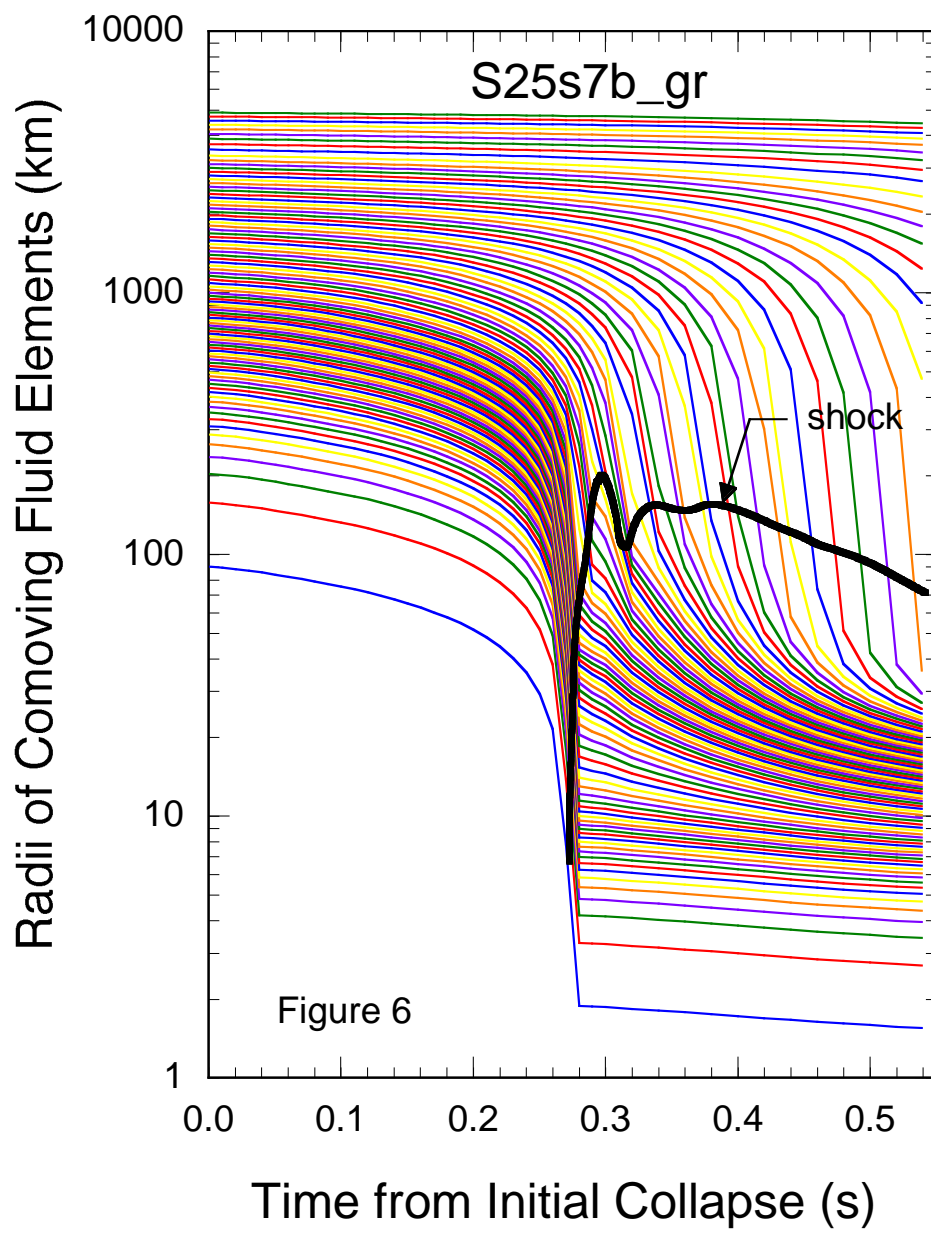


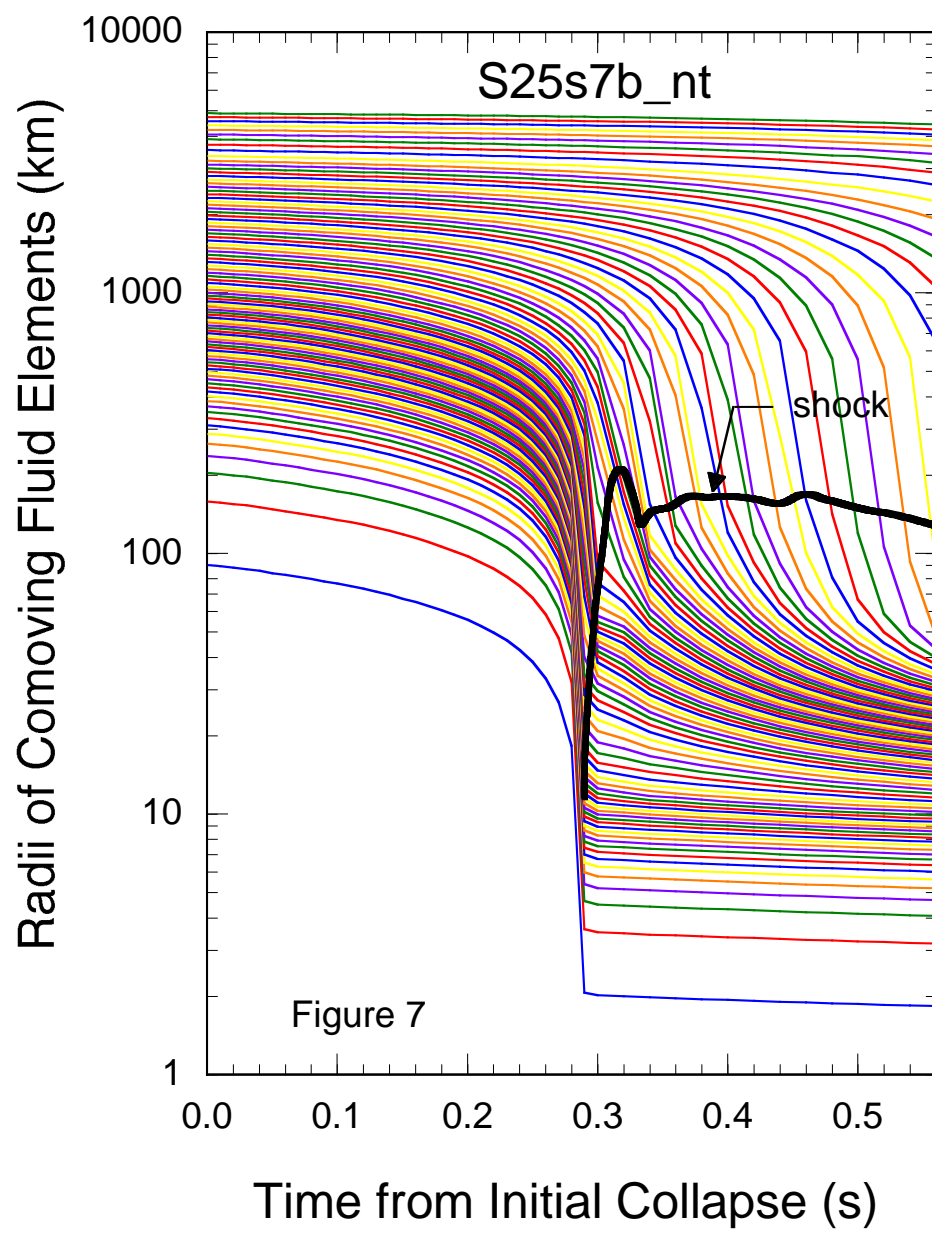


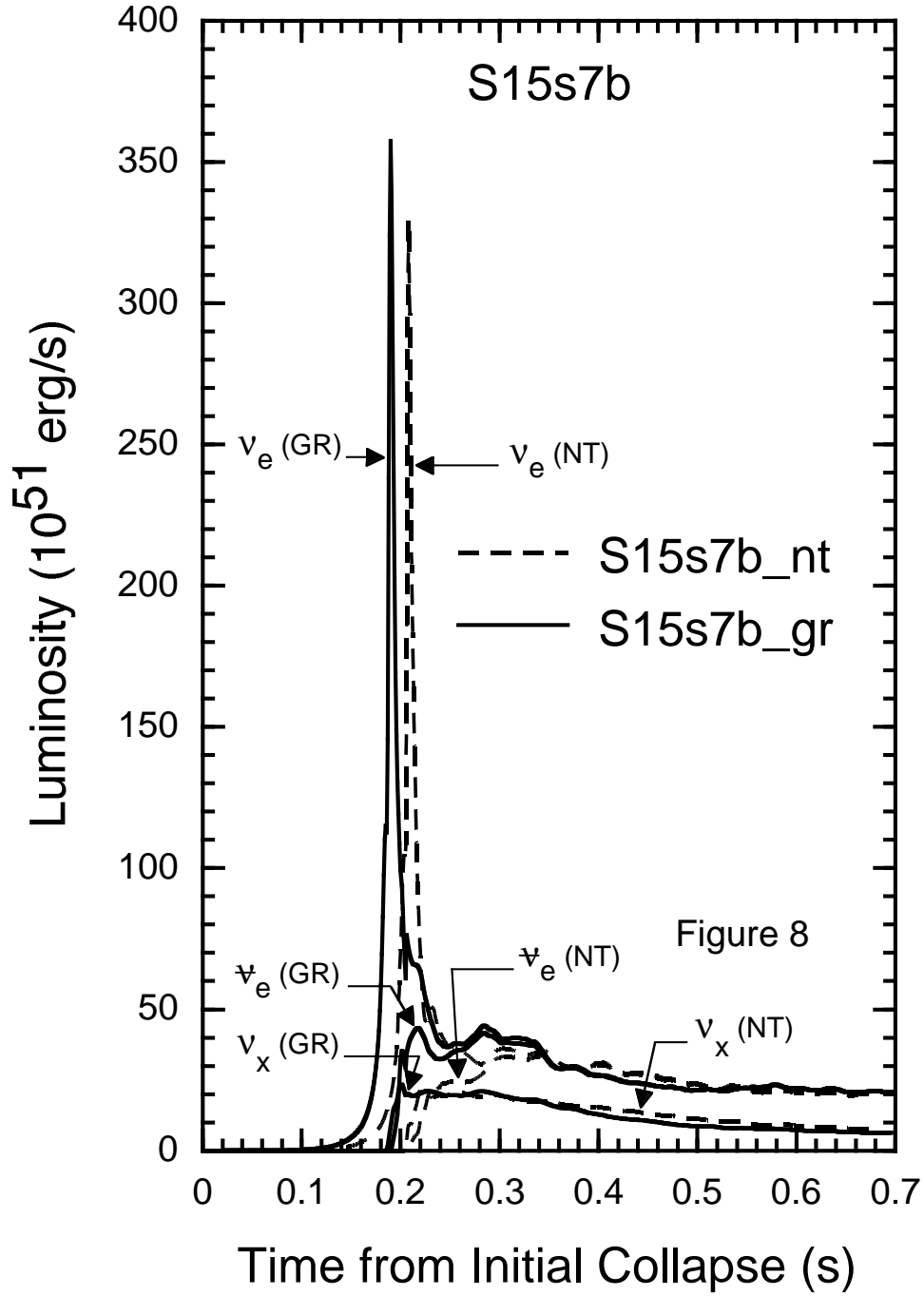


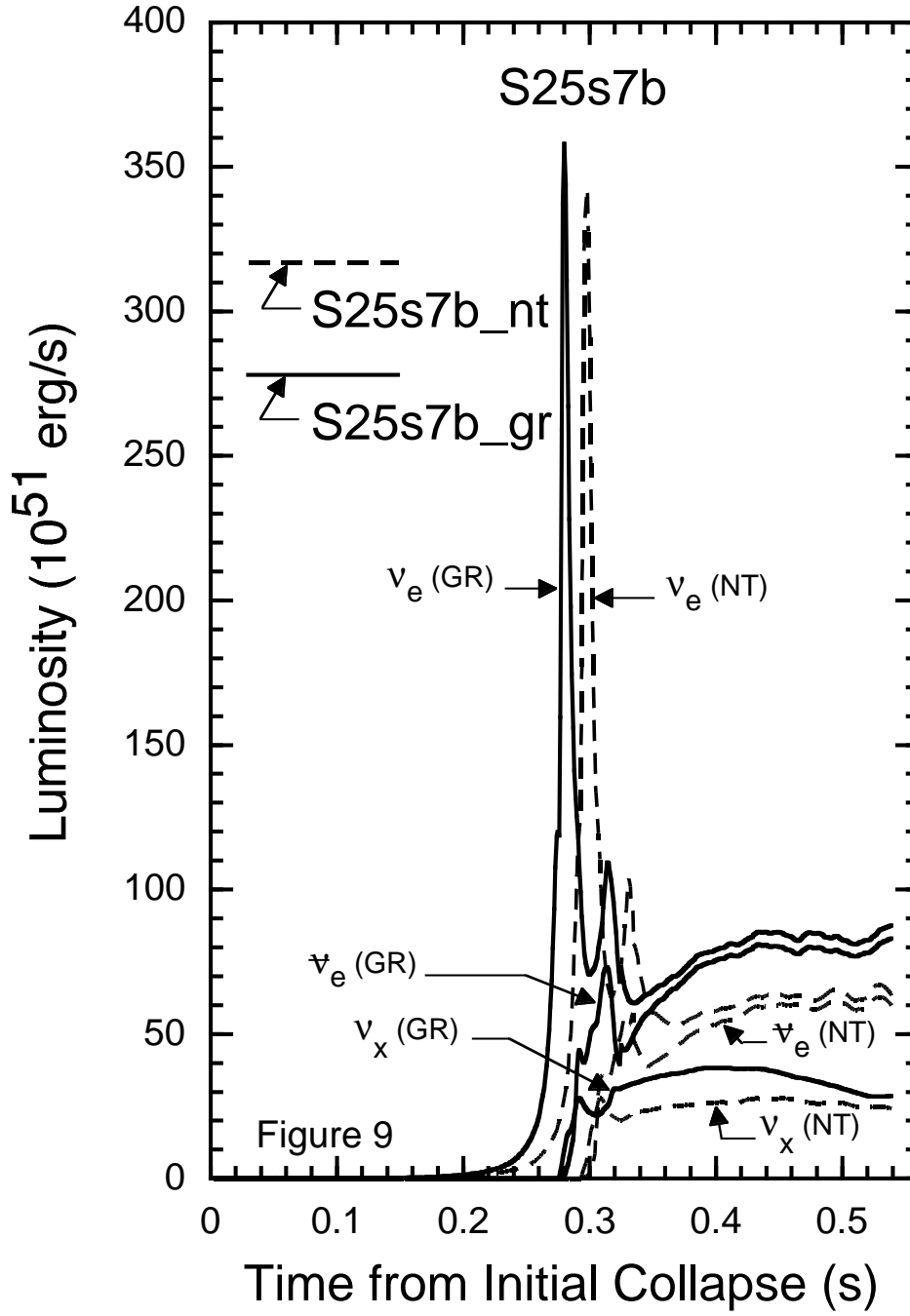


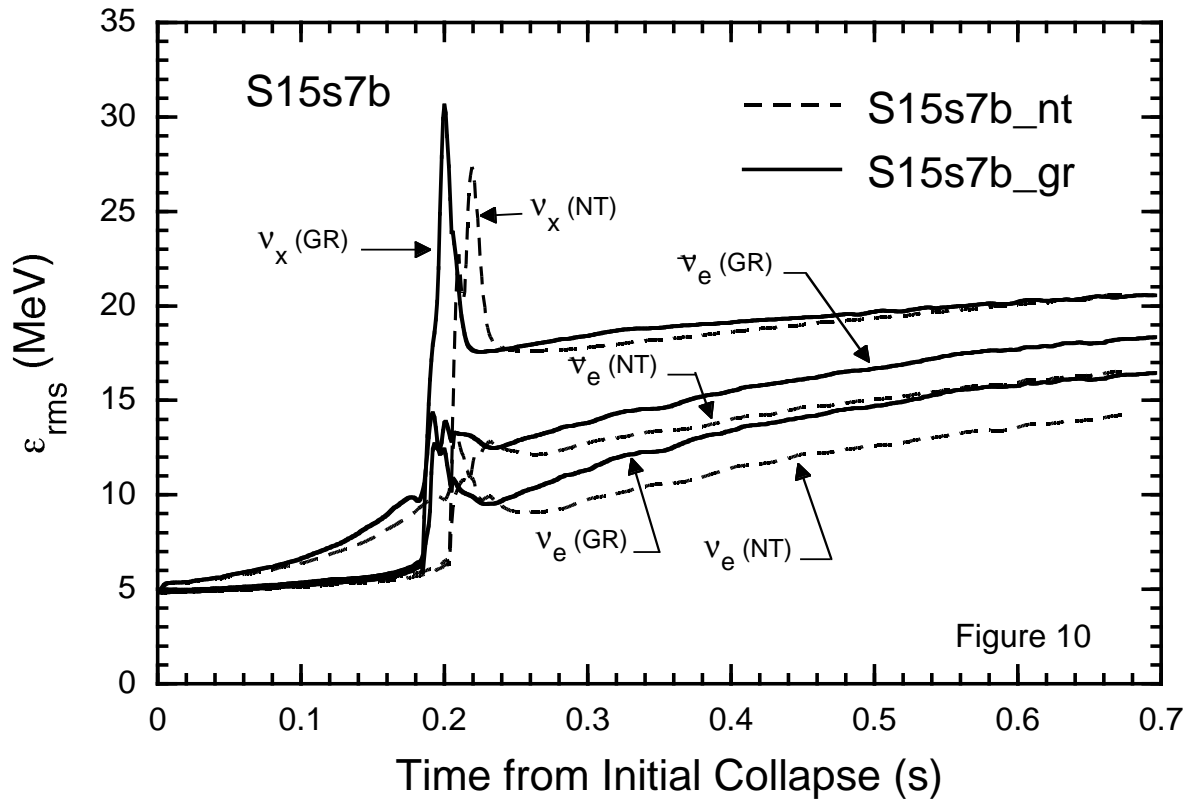


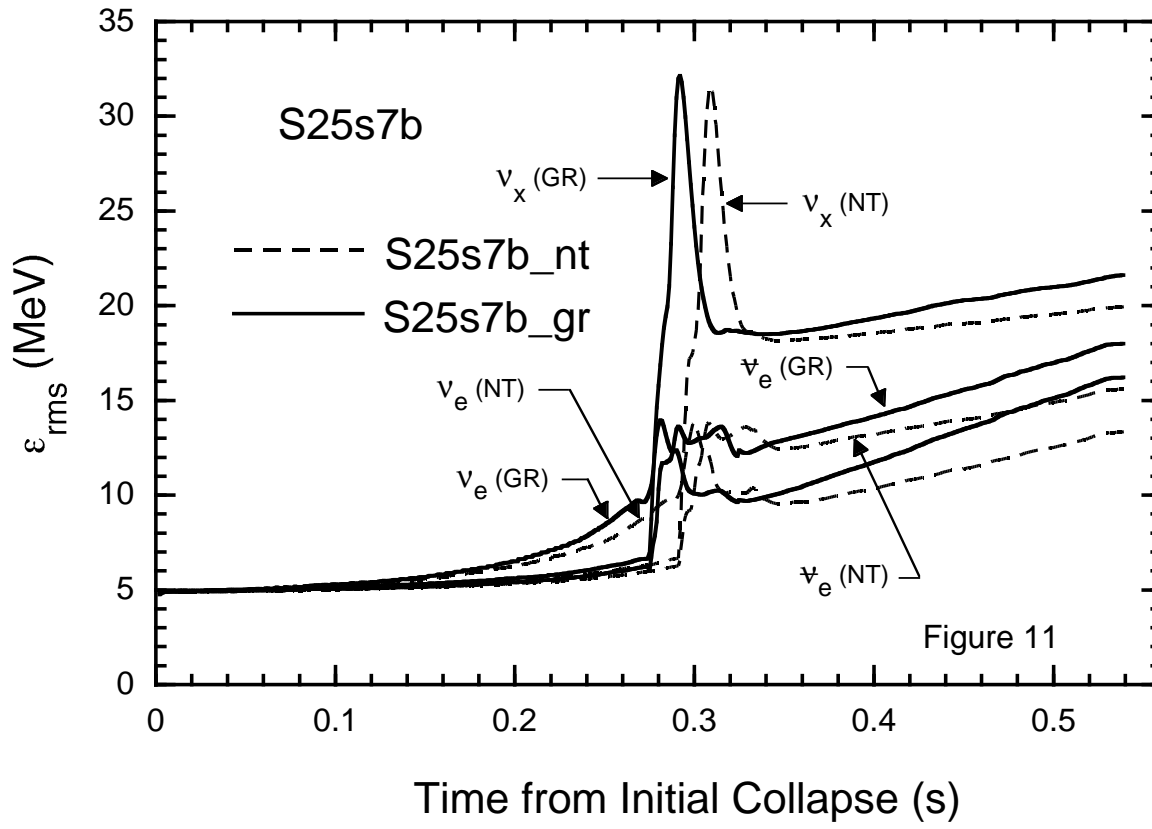












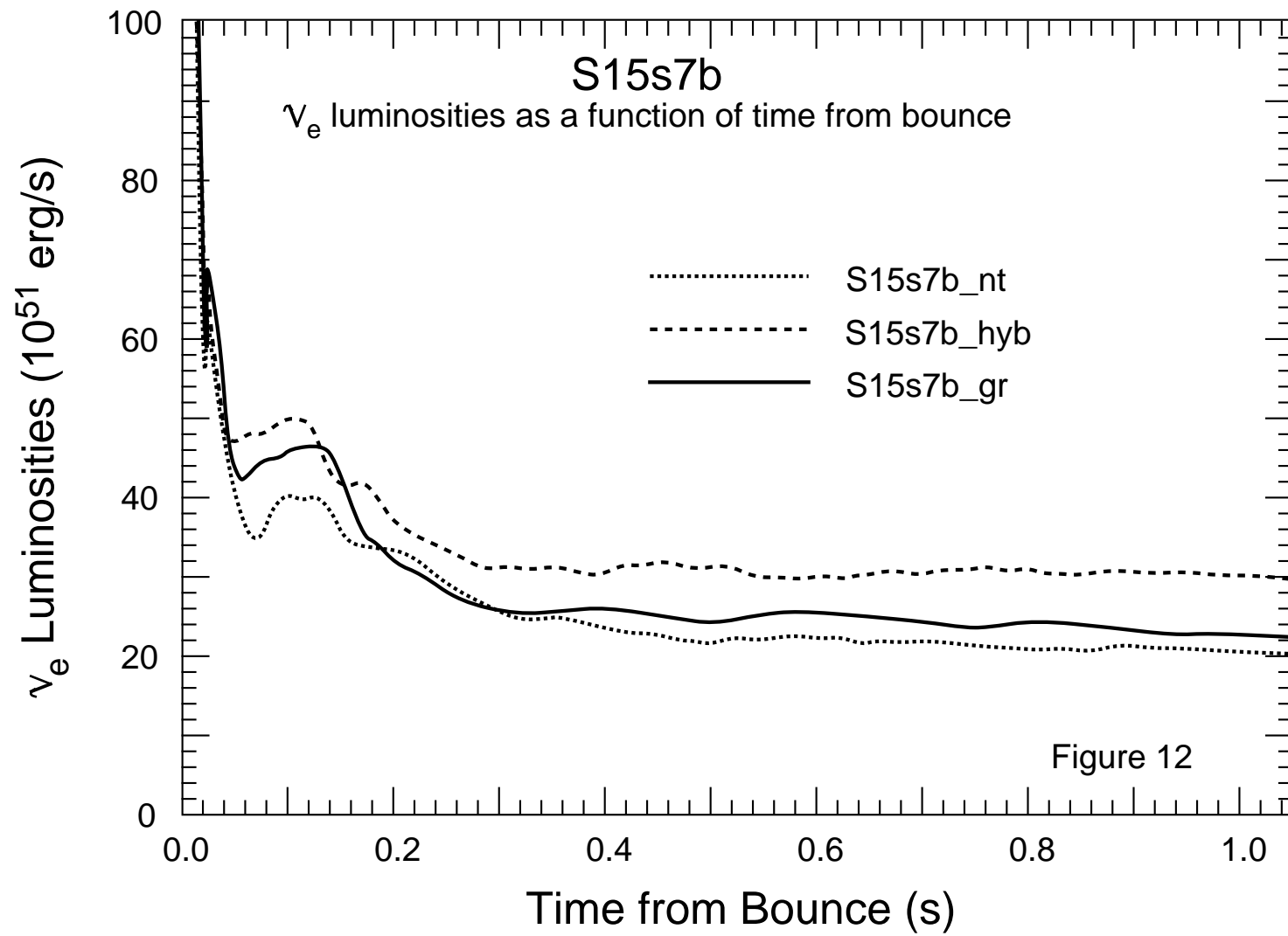
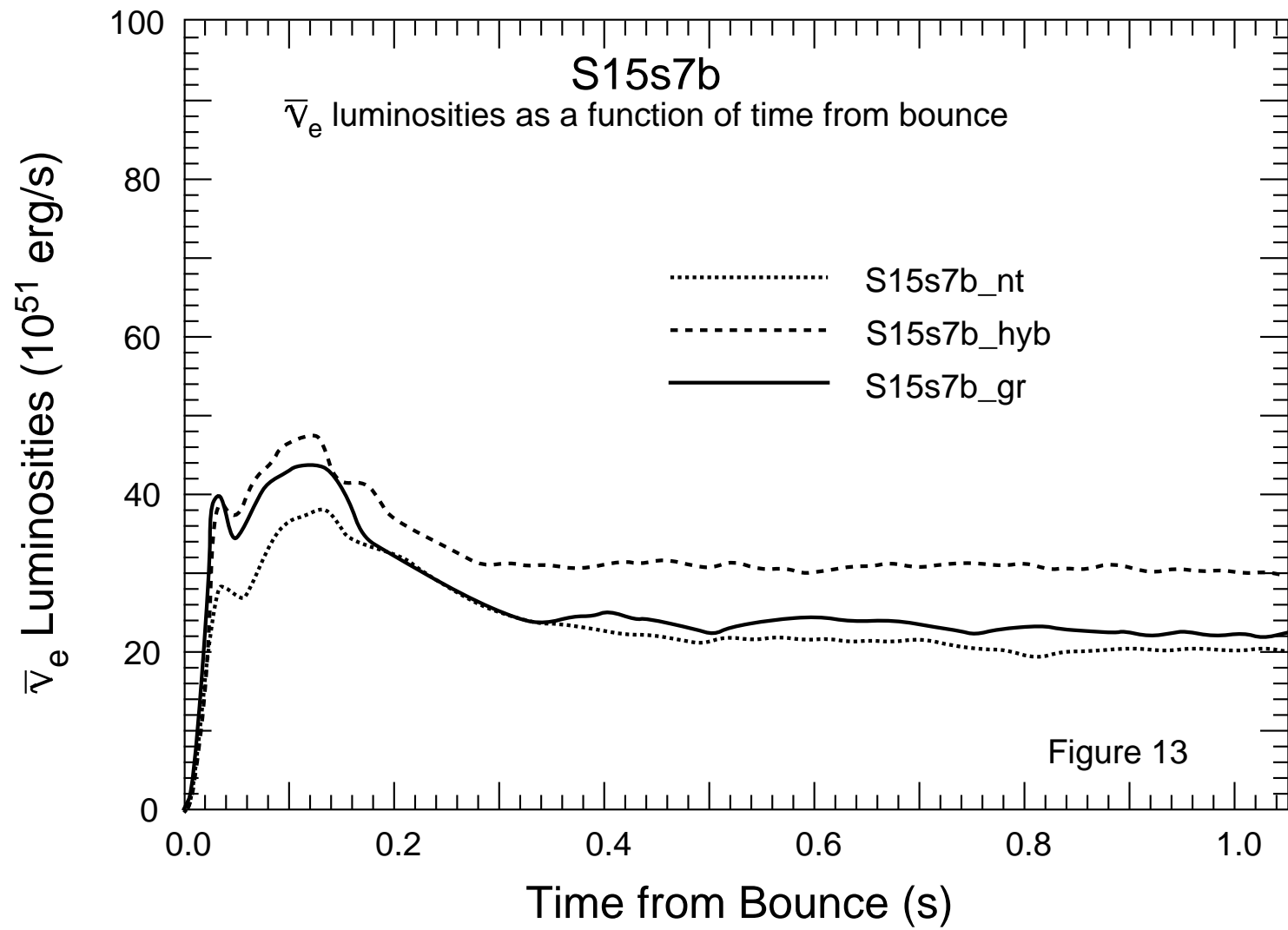
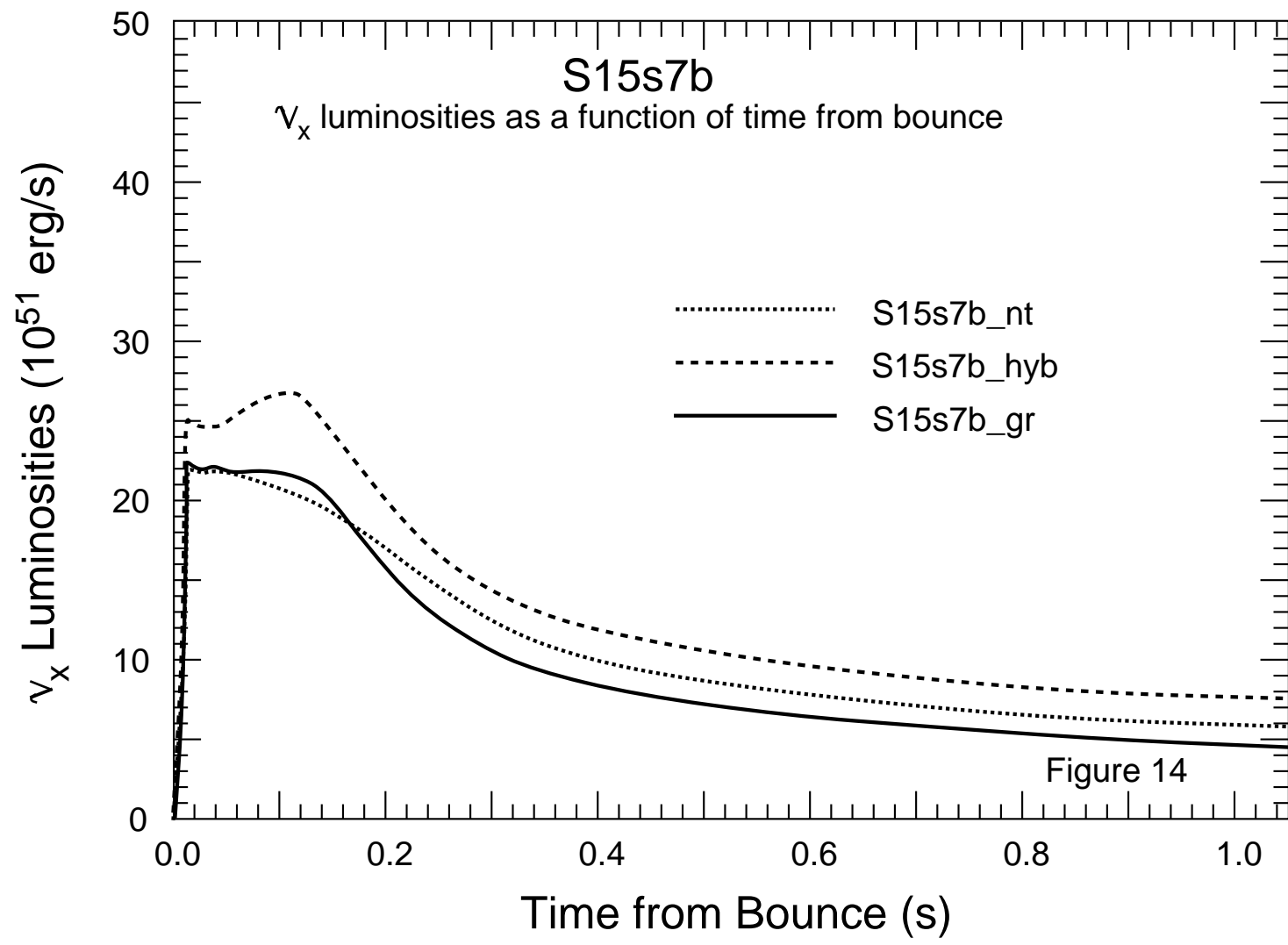


Figure 12





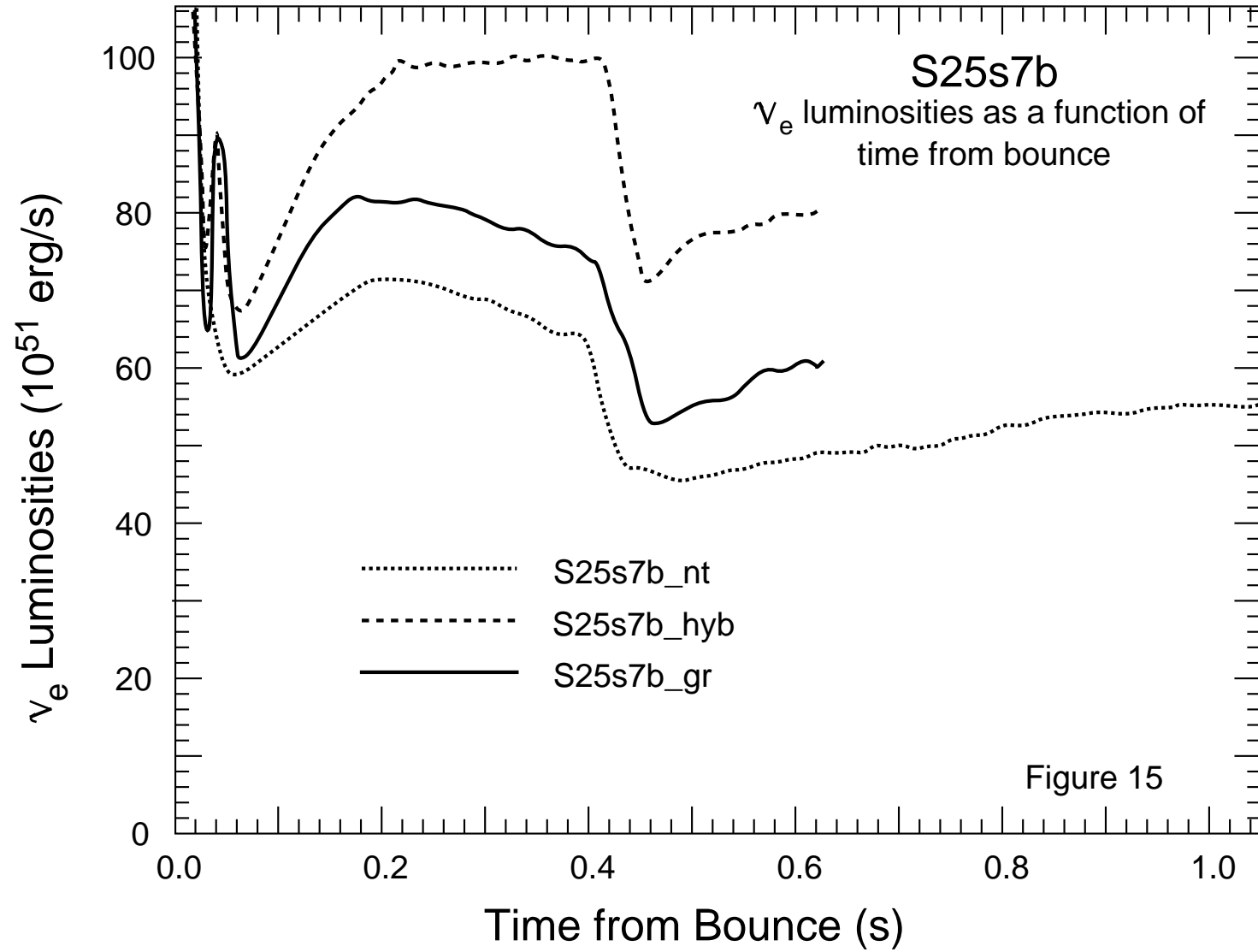


Figure 15

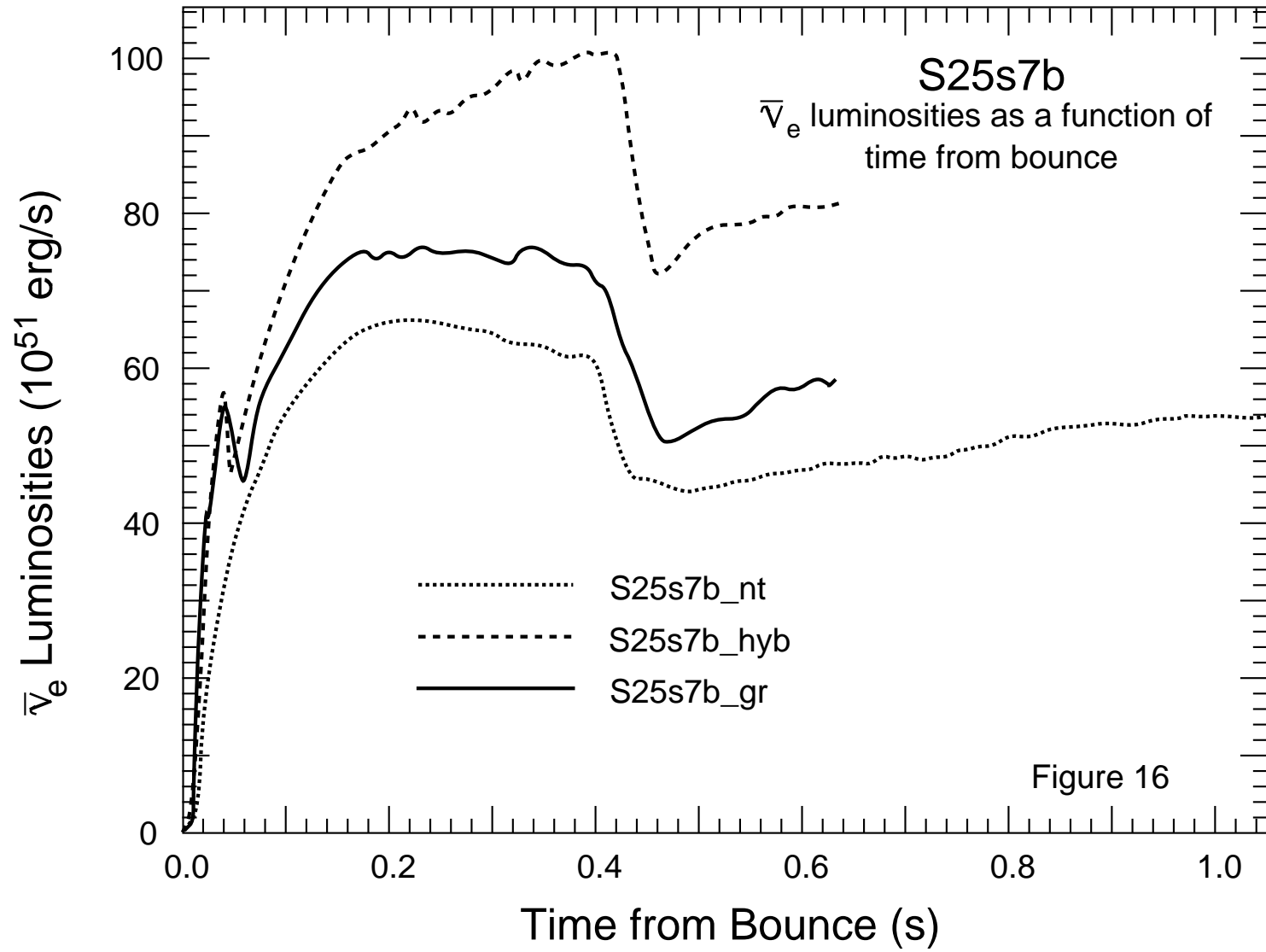


Figure 16

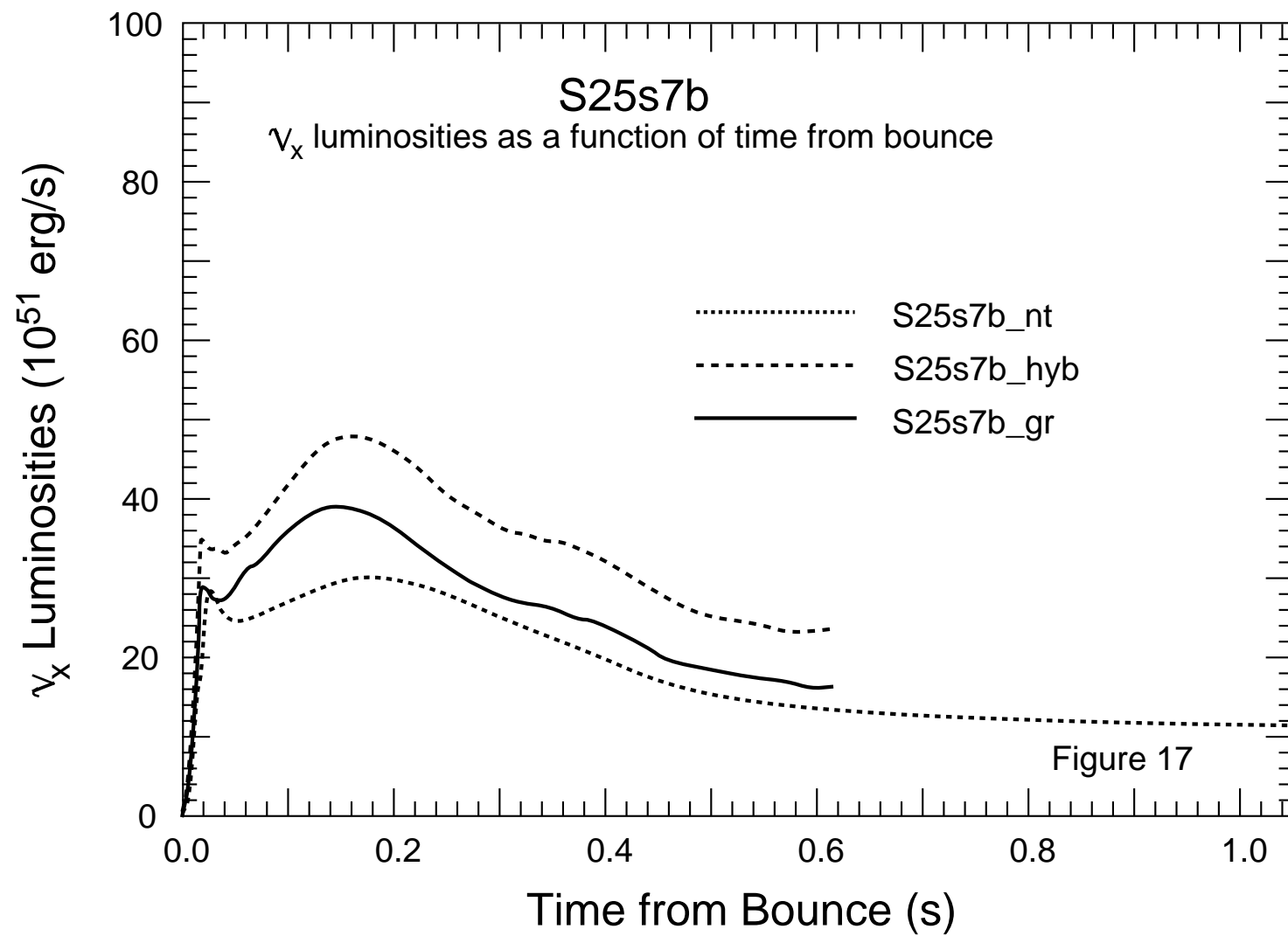


Figure 17

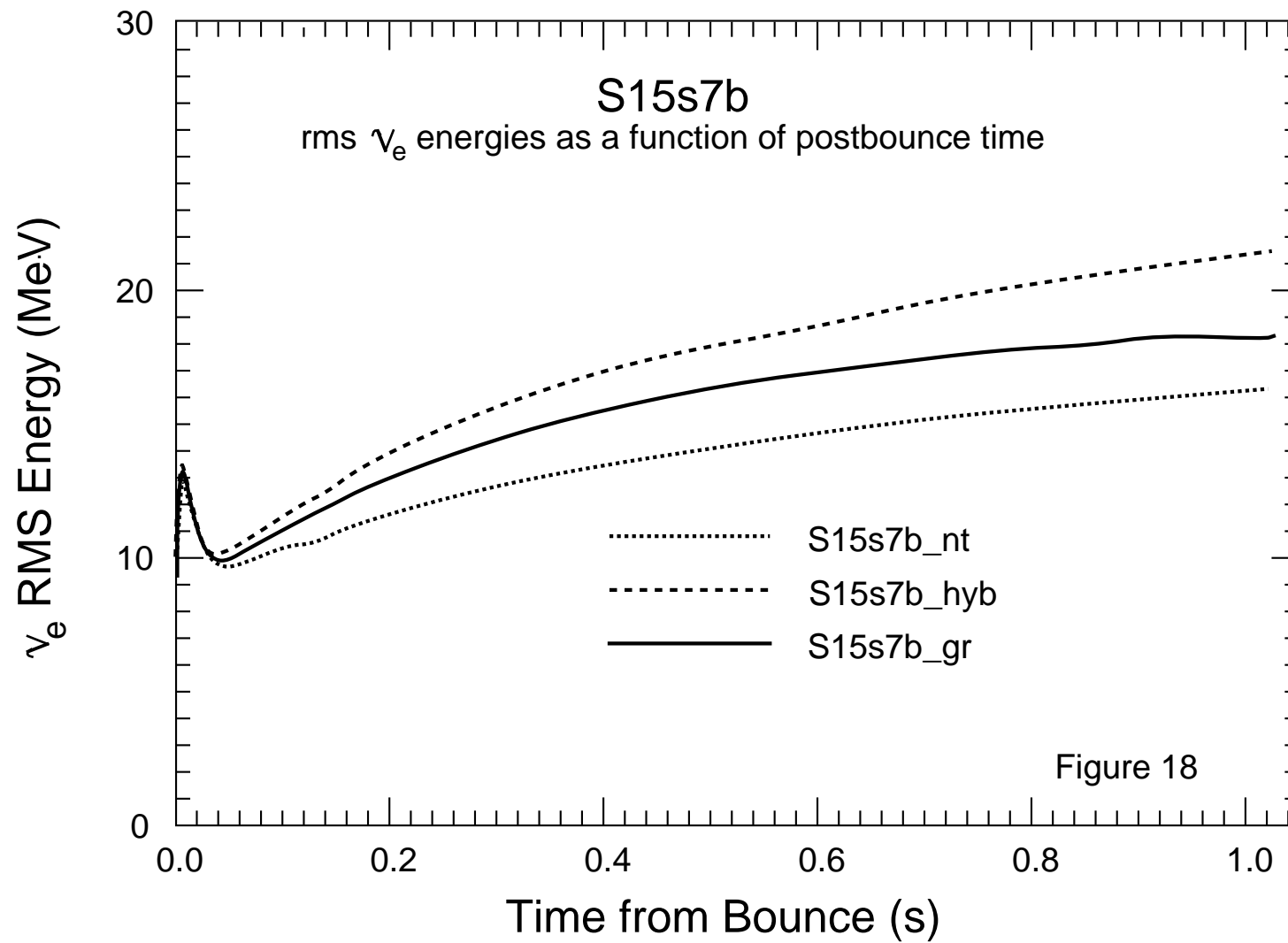


Figure 18

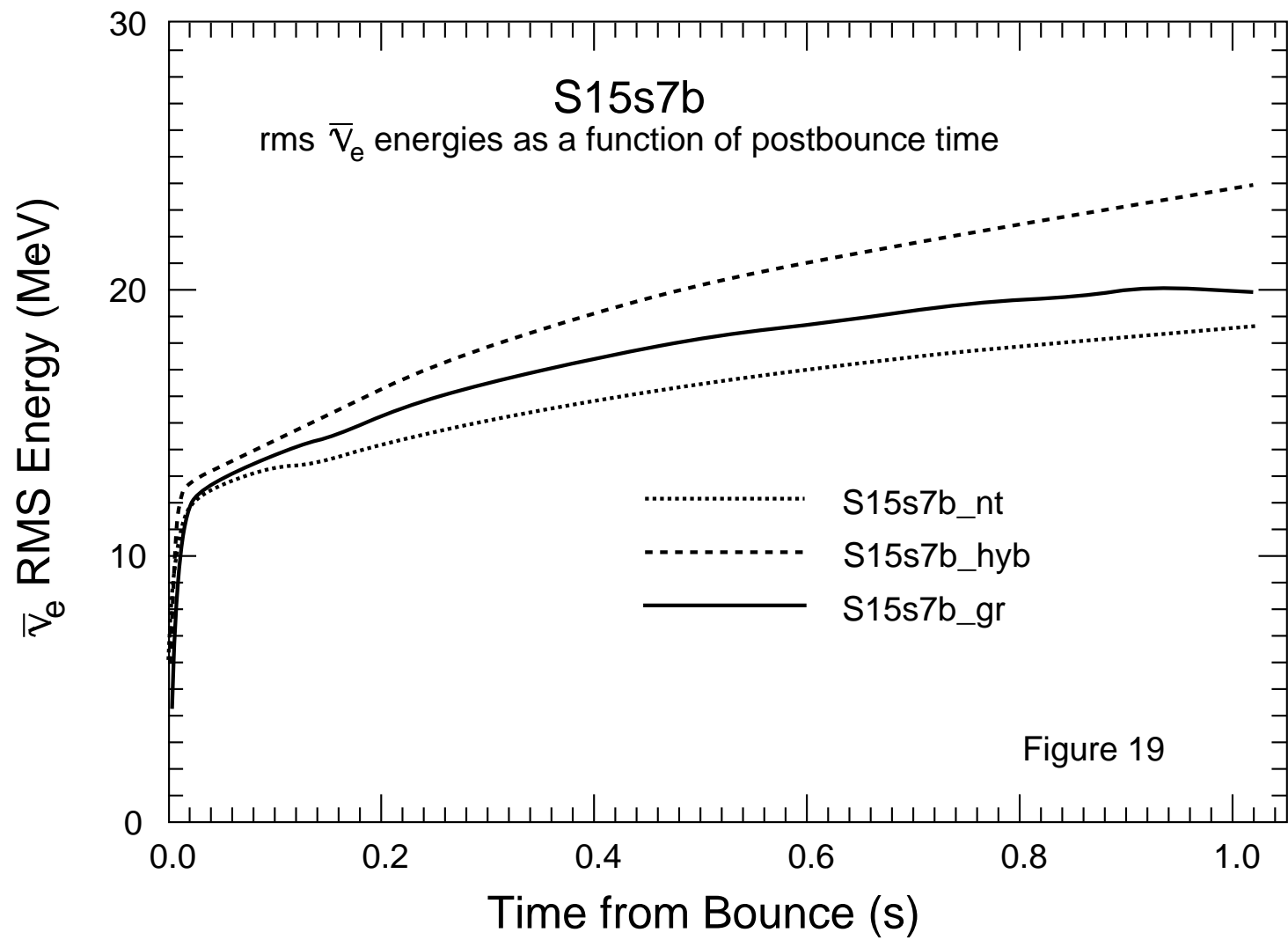


Figure 19

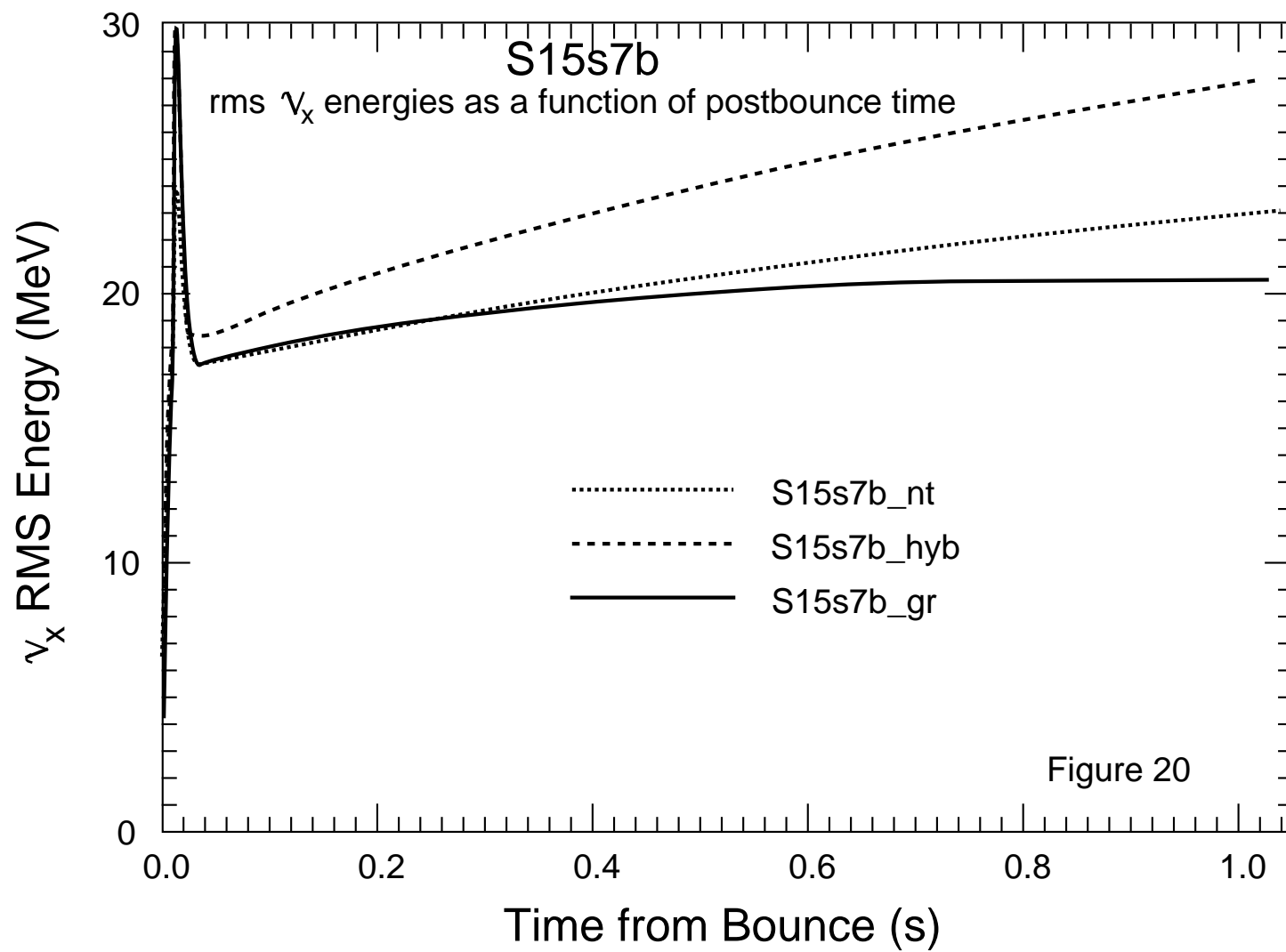


Figure 20

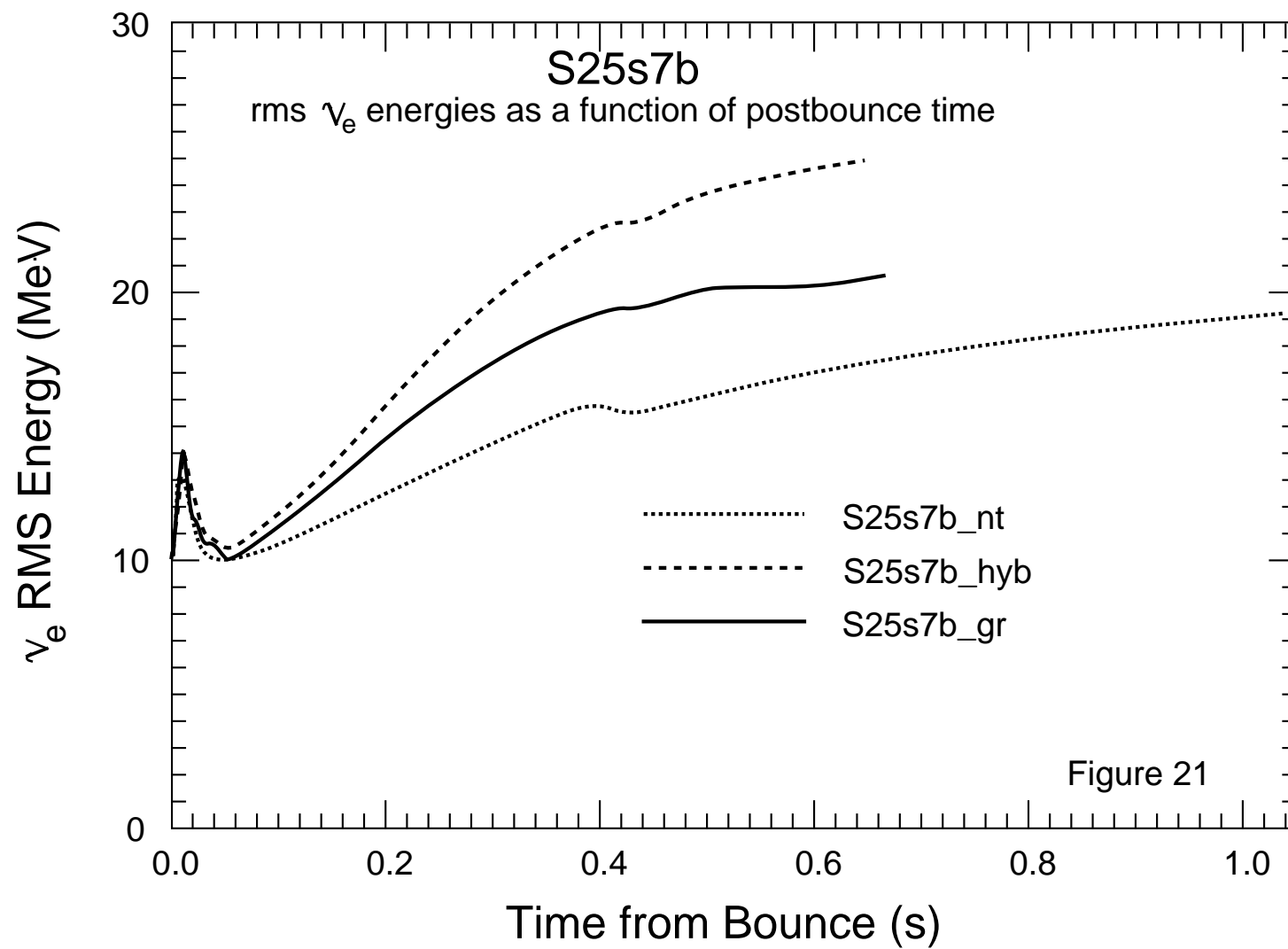


Figure 21

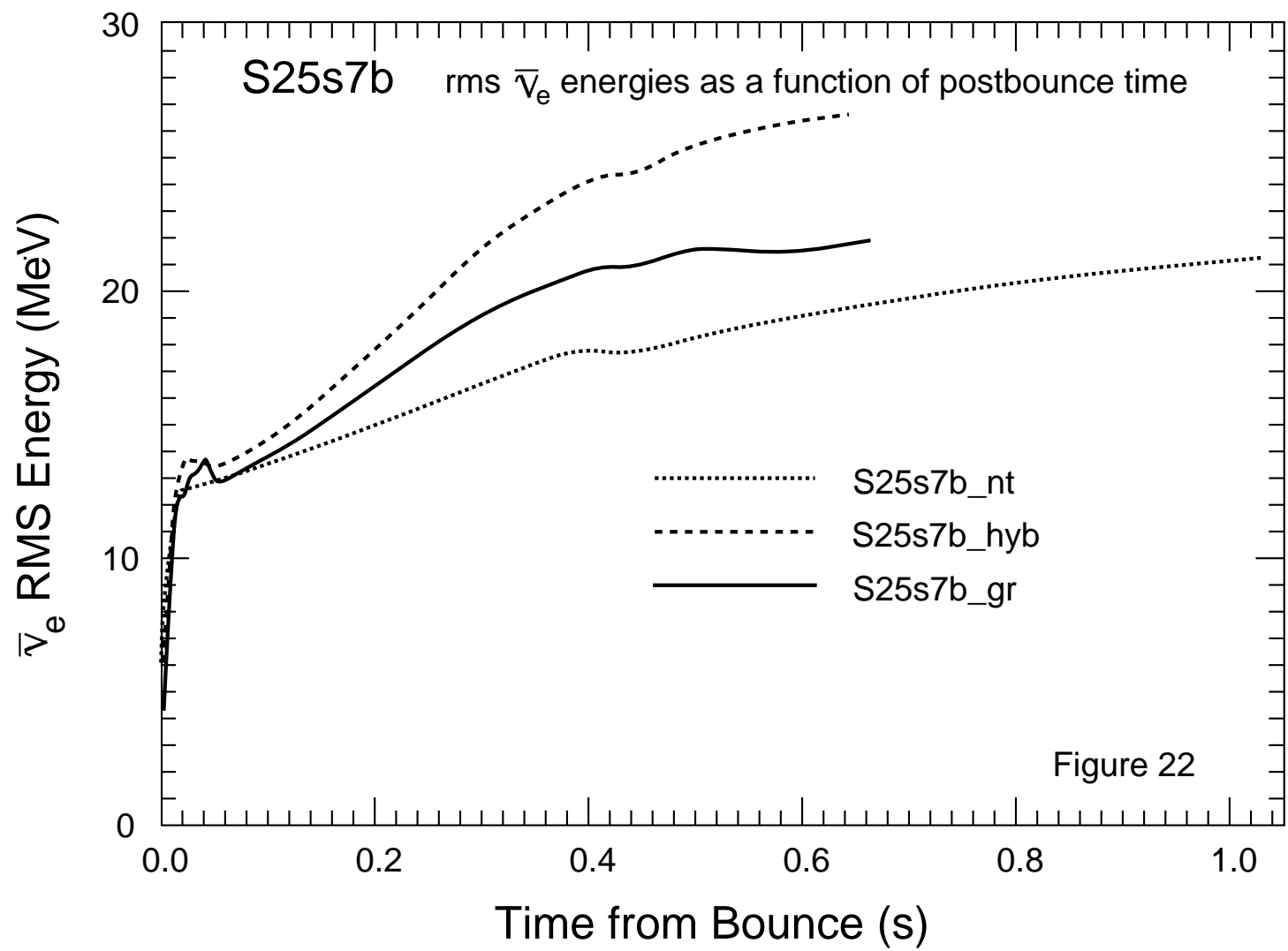


Figure 22

